General Disclaimer

One or more of the Following Statements may affect this Document

- This document has been reproduced from the best copy furnished by the organizational source. It is being released in the interest of making available as much information as possible.

- This document may contain data, which exceeds the sheet parameters. It was furnished in this condition by the organizational source and is the best copy available.

- This document may contain tone-on-tone or color graphs, charts and/or pictures, which have been reproduced in black and white.

- This document is paginated as submitted by the original source.

- Portions of this document are not fully legible due to the historical nature of some of the material. However, it is the best reproduction available from the original submission.

NASA TECHNICAL MEMORANDUM

NASA TM X-71746

NASA TM X-71746

(NASA-TM-X-71746) THE EFFECT OF CIRCUMFERENTIAL DISTORTION ON FAN PERFORMANCE AT TWO LEVELS OF BLADE LOADING (NASA) 29 p HC $3.75 CSCL 21E

N75-25947

Unclas
G3/07 26678

THE EFFECT OF CIRCUMFERENTIAL DISTORTION ON FAN PERFORMANCE AT TWO LEVELS OF BLADE LOADING

by Melvin J. Hartmann and Nelson L. Sanger
Lewis Research Center
Cleveland, Ohio 44135

TECHNICAL PAPER to be presented at
Forty-fifth Meeting of the Propulsion and Energetics Panel sponsored by AGARD
Monterey, California, September 22-26, 1975

THE EFFECT OF CIRCUMFERENTIAL DISTORTION ON FAN PERFORMANCE AT TWO LEVELS OF BLADE LOADING

by
Melvin J. Hartmann, Chief, Fan and Compressor Branch,
and Nelson L. Sanger, Research Engineer
Lewis Research Center
National Aeronautics and Space Administration
Cleveland, Ohio 44135

SUMMARY

Single stage fans designed for two levels of pressure ratio or blade loading (rotor tip D-factor of 0.43 and 0.54) were subjected to screen-induced circumferential distortions of 90-degree extent. Both fan rotors were designed for a blade tip speed of 425 m/sec, blade solidity of 1.3 and a hub-to-tip radius ratio of 0.5. Circumferential measurements of total pressure, temperature, static pressure, and flow angle were obtained at the hub, mean and tip radii at five axial stations (three between the screen and rotor and behind rotor and stator blade rows).

E-8385

Rotor loading level did not appear to have a significant influence on rotor response to distorted flow. Losses in overall pressure ratio due to distortion were most severe in the stator hub region of the more highly loaded stage. At the near stall operating condition tip and hub regions of (either) rotor demonstrated different response characteristics to the distorted flow. No effect of loading was apparent on interactions between rotor and upstream distorted flow fields.

SYMBOLS

D	diffusion factor
i_{ss}	incidence angle, angle between inlet air direction and a line tangent to the blade suction surface at the leading edge, deg
M_1, M_2, M_{ss}	Mach number at rotor inlet, stator inlet, and peak blade suction surface
N	rotative speed, rpm
P	total pressure, N/cm^2
PR	pressure ratio; P_2/P_1 (rotor), P_3/P_1 (stage)
ΔPRS	loss of surge pressure ratio, $\frac{PR_{undist} - PR_{dist}}{PR_{undist}}$
p	static pressure, N/cm^2
r	radius, cm
T	total temperature, K
V_θ, V_z	tangential and axial velocity
X-factor	ratio of suction surface camber ahead of assumed shock location of a multiple circular arc blade section to that of a double circular arc blade section
z	axial distance, cm
η	adiabatic (temperature-rise) efficiency
θ	circumferential location, deg
$\bar{\omega}$	total loss coefficient

Subscripts:

M.S.	mid-span radial location
-1,0,1,2,3	measuring station axial positions (Fig. 2)

Superscripts:

'	relative to blade
¯	average

1.0 INTRODUCTION

One of the most difficult problems in fluid mechanics is the analysis of flow through a fan or compressor having circumferential variations in inlet flow properties. Imposed on all the customary aerodynamic complexities of turbomachinery flow, a circumferentially distorted inlet flow introduces a strong three-dimensional flow component which is seen as unsteady by the rotor (in the relative flow field) and

as steady by the stator. Theoretical models are not sufficiently developed to analyze such flow fields.

Consequently, systematic experimental programs are currently necessary to provide insight into the aerodynamics and permit more distortion-tolerant designs to be evolved. Distortion measurements are taken as part of a general program of fan and compressor research conducted by the Fan and Compressor Branch at the Lewis Research Center. Attention is concentrated on "steady-state" distortion patterns (the magnitude and extent are nonfluctuating with time) which are produced experimentally by wire mesh screens.

Fan and compressor designs incorporating higher tip speeds and higher blade loadings have been required to meet the needs of advanced propulsion systems. The question arises as to whether these high performance fans and compressors are as tolerant to distortion as earlier designs. In a previous investigation of two single rotors (no stator row) having different levels of loading (Ref. 1), the higher loaded rotor did not appear to incur greater losses in performance under circumferentially distorted inlet flow. However, the full question of the effect of circumferential distortion and loading level was left unresolved because no distinct stall point could be established, and because full stage testing was not included in the investigation.

In this paper the performance of two low hub-to-tip radius ratio (0.5) transonic fan stages (single stage) with inlet flow distorted by a 90-degree extent wire mesh screen are compared. Both were designed for the same equivalent flow rate (29.5 kg/sec) and tip speed (425 m/sec), but for different stage pressure ratios (1.57 and 1.75). Aerodynamic performance with undistorted flow was presented in Refs. 2 and 3, respectively. Detailed performance with circumferentially distorted flow was discussed in Ref. 4 for the 1.57 pressure ratio stage. The objective of the study is to evaluate the aerodynamic performance, under circumferentially distorted inlet conditions, of two fan stages having different loading levels; and to determine the reasons for any performance differences which may be attributable to loading.

In exploring these questions, pertinent design features of the blading in each stage will be presented. Overall performance of each stage will be compared with each other and with performance under undistorted inlet conditions. Detailed flow measurements around the circumference at three radial positions were made between the distortion screen and the rotor inlet, and are evaluated to determine the degree of interaction between the rotor and the upstream distorted flow field. Similar detailed flow measurements were made at rotor and stator exit planes to determine the stage response to the imposed distortion. Detailed data are examined at the near stall condition for design speed. Overall performance with distortion is also presented for 70% of design speed.

2.0 APPARATUS AND PROCEDURE

The apparatus to be discussed consists of the test facility, instrumentation, and distortion screens. A description of these items will be followed by a discussion of test and calculation procedures. Finally, the design features of both fan stages will be presented and compared.

2.1 Test Facility

The tests were conducted in the Lewis single-stage compressor facility. A schematic diagram of the facility is presented in Fig. 1 and a complete description in Ref. 5. Air enters the system through an inlet on the roof, passes through a measuring orifice, and into the plenum. It then passes through the distortion screens, the test stage, and into a collector from which it is exhausted to the atmosphere. Back pressure on the stage is controlled by a slide valve located in the collector. All tests were conducted with atmospheric inlet conditions.

2.2 Instrumentation

Compressor flow rate was measured using a calibrated thin-plate orifice located in the inlet piping as shown in Fig. 1.

Radial surveys of the flow were made at five axial locations, three of which were upstream of the rotor. A schematic figure of the flow paths and survey locations is shown in Fig. 2. The type of probe used to obtain the survey data is shown in Fig. 3 and reported in Ref. 6. For these distortion tests, where it was thought desirable to obtain all measurements at the same location, static pressures were obtained by averaging the pressures measured from the taps on the two sides of the 60 degree wedge and utilizing calibration curves relating these readings with true static pressures. Accuracy is not as high as could be obtained through use of the conventional small angle static wedge. However, emphasis in interpretation is placed on changes which occur between undistorted flow and distorted flow, or on changes between two different distorted flow conditions, rather than on direct comparisons of absolute values of any single parameter.

All pressures were transmitted through a Scanivalve System and measured by calibrated transducers.

2.3 Distortion Screens

The distortion screen assembly used in the investigation was located 36.25 cm upstream of the rotor hub leading edge. The assembly was rotated to twelve circumferential positions to obtain the distortion patterns measured by a single survey probe.

A 20 × 20 wire mesh (20 wires per 1 in. or 2.54 cm) was used. Wire diameter was 0.051 cm, resulting in a 36 percent open area. A 90 degree nominal circumferential distortion extent was chosen for general research testing because this is generally of sufficient width to affect performance, and is representative of actual flight application extents. The distortion screen was secured to a backup screen having a 1.9 × 1.9 cm clear opening and a 0.27 cm wire diameter. The screen was sized to produce a 90-degree distortion at rotor inlet and, due to interaction effects between rotor and upstream flow, this

resulted in a screen having extents of 85 degrees at the outer radius and 135 degrees at the inner radius. A photograph of the assembly is shown in Fig. 4.

Rotor rotational speed was measured by an electric speed counter which sensed pulses from a magnetic pickup.

A further discussion of the instrumentation may be found in Ref. 4.

2.4 Test Procedure

With only the backup screen in place (reference undistorted inlet flow condition) radial surveys were taken for both stages over a range of weightflows from maximum flow to the near stall condition at 70 and 100 percent of design speed. At 60, 80, and 90 percent of design speed surveys were taken only at the near stall weight flow. Data were recorded at 11 radial positions for each operating condition.

At each speed the back pressure, with and without distortion, was increased by closing the outlet valve until a stalled condition was obtained. Stalled or surge conditions were indicated by a sudden drop in stage outlet pressure (measured by a mid-passage monitoring probe and recorded on an X-Y plotter), by large increases in measured blade stresses on both rotor and stator, and by a sudden increase in audible noise level. Radial survey data were taken at a weight flow as close to actual stall as practical. In general, this was within 0.5 kg/sec of the actual stall weight flow.

For the circumferential distortion tests on both stages radial survey data were taken only at 100 and 70 percent of design speed. At 100 percent speed, data were taken over a range of weightflows from near stall to maximum weight flow; at 70 percent speed, data were taken at near stall for both stages and also at midflow for the lower pressure ratio stage. Survey data were recorded at three radial positions: 10, 45, and 90 percent span from the tip. A radial survey was taken at each of the twelve screen positions.

2.5 Calculation Procedure

All data presented in this report have been adjusted to standard conditions (total pressure of 10.13 N/cm^2 and total temperature of 288 K) at the rotor inlet (station 1). The term equivalent when applied to weight flow or speed refers to corrected values of these parameters. The calculation procedure used for undistorted tests with backup screen in place (designated BUS) is the same as used for conventional clean inlet tests and is given in Ref. 2. The following discussion applies to the calculation procedure used for circumferential distortion data.

Measured total temperature, total pressure, and static pressure were corrected for Mach number and streamline slope according to the procedure given in Ref. 4. Before adjustment to standard conditions circumferential distortion data is mass-averaged circumferentially and radially. No blade element performance parameters were calculated because of the asymmetric nature of the flow, which, in the rotor relative flow plane, is unsteady. For the same reasons the data were not translated from the measuring station to blade edge planes.

To obtain overall total temperature and pressure ratios, the twelve circumferential values were mass-averaged at each radial position, and the three radial values were then mass-averaged. Integrated weight flow was computed at each station based on radial survey data.

For axisymmetric inlet flow, as reported in Ref. 2, eleven radial positions are measured and used in the averaging process. However, to permit direct comparison of backup screen data and circumferential distortion data, only the three radial positions corresponding to those taken for distorted flow will be used in the averaging process for BUS data.

2.6 Single Stage Fans

2.6.1 General Description

A comparison of the pertinent design features of each single stage fan is presented in Table I. The stage designed for a pressure ratio of 1.57 is designated Stage 11-4 (rotor 11, stator 4) and the higher pressure ratio stage is designated Stage 14-10. It should be noted that both stages were designed for the same flow rate, rotor tip speed (same nominal rotor tip radius of 25.4 cm), and same rotor and stator tip solidities. Because Stage 14-10 was designed to produce a higher pressure ratio at the same rotor tip speed, D factors are higher (measure of blade loading). Flow paths also differ, principally in the stator hub region (Fig. 2). Rotor and stator blade shapes were multiple-circular-arcs (MCA) for both stages. Each rotor had vibration dampers. They were located at about 48 percent span from the rotor outlet tip on rotor 11 and 50 percent on rotor 14.

2.6.2 Aerodynamic Design

Tabular listings of design blade element parameters and blade geometry are presented for each stage in Refs. 2 and 3. Radial distributions of geometry and aerodynamic parameters selected for comparison herein are those which are pertinent to the subsequent discussion of aerodynamic performance with distortion.

Design distributions of total pressure ratio, D-factor and total loss coefficient for each rotor are compared in Fig. 5. Both rotors were designed for radially constant distributions of total pressure. Distributions of D-factor are similar for both rotors, differing only in magnitude and reflecting the difference in design pressure ratio. Loss distributions are quite similar in distribution and magnitude for both rotors. The high levels of loss in the tip region reflect both the end wall boundary layer contribution and the shock losses (relative Mach number at the tip is 1.4 for both rotors).

Two related stator blade geometry parameters are compared in Fig. 6(a), X-factor and throat area

ratio. X-factor is defined as the ratio of suction surface camber ahead of the assumed shock location for the MCA section to that of a double circular arc section. This parameter was increased almost linearly from midspan to the hub for stator 10, in order to prevent the throat area ratio at these blade sections from decreasing to a level which would cause the hub region to choke. Because of the higher fluid turning necessary in Stage 14-10 the D-factor levels are higher (Fig. 6(b-1)) as are inlet Mach numbers (Fig. 6(b-2)). The higher inlet Mach numbers and higher front turning (X-factor) in the hub region leads to higher peak suction surface Mach numbers (Fig. 6(b-3)) in that region. And because of the higher Mach numbers and D-factor, Stator 10 loss levels are greater than Stator 4 losses at all radial positions (Fig. 6(b-4)).

3.0 RESULTS AND DISCUSSION

The effect of circumferential distortion on the performance of two fan stages in which aerodynamic loading (pressure ratio) is the primary variant will be presented in three sections:

(1) Overall rotor and stage performance

(2) Rotor-upstream flow interactions

(3) Circumferential flow distributions

The magnitude of inlet flow distortion, $(P_{max} - P_{min})/P_{max}$, at design speed, near stall condition was 0.12 at the mean radius, and was about one-third this magnitude at 70 percent of design speed.

3.1 Overall Rotor and Stage Performance

Overall performance maps for rotor and stage performance are presented in Fig. 7 for Stage 11-4 and in Fig. 8 for Stage 14-10. Efficiency and pressure ratio are plotted as a function of weight flow for performance with undistorted flow (BUS) and circumferentially distorted inlet flow.

Operation with circumferentially distorted flow resulted in lower rotor and stage pressure ratio over the entire operating range at design speed for each fan stage. The difference between BUS and circumferential distortion design speed lines for the full Stage 11-4 is slightly less than the difference for the rotor (11), which indicates that losses through stator 4 were probably slightly less with distortion than without. The opposite is true for Stage 14-10. Losses through stator 10 are significantly higher with distorted flow than without. Also, differences in rotor performance from BUS levels are less for rotor 14 than for rotor 11.

At 70 percent of design speed there is little difference between BUS and distorted flow speed lines for rotor 11 and Stage 11-4. But even though rotor 14 shows the same negligible effect of distortion at 70 percent speed, the stage shows a lower pressure ratio with distortion, indicating higher stator losses at this speed also.

Both stages suffered a slight decrease in maximum flow attained with distortion at design speed. No particular conclusion should be drawn from the efficiencies because of the difficulty associated with mass-averaging distorted inlet and outlet flows (with only three radial positions represented), and the sensitivity of efficiency to small changes in value of either temperature ratio or pressure ratio.

The change in stall pressure ratio from BUS to circumferentially distorted flow indicated on the figures is summarized in Table II. The pressure ratio at near stall for BUS and circumferentially distorted flow is presented and the loss of stall pressure ratio as a proportion of the undistorted near stall pressure ratio is given as ΔPRS (see definition in SYMBOLS section). "Pressure ratio at near stall" refers to the pressure ratio measured when stage stall occurred. The loss in stall pressure ratio due to distortion in Stage 11-4 is sustained principally by the rotor at design speed. No further degradation due to distortion (measured by ΔPRS) occurs in the stator. At 70 percent of design speed stall pressure ratio is essentially unaffected by circumferential distortion. Stage 14-10 displays a different response. At design speed a 4 percent loss in stall pressure ratio occurs in the rotor and this loss is more than doubled through the stator. At 70 percent of design speed the rotor shows no loss in stall pressure ratio, but the stage (and therefore, the stator) does.

A direct comparison of pressure ratio versus weight flow performance curves for both stages is shown in Fig. 9. The large loss in pressure ratio in stator 10 is evident.

In summary, for the two stages under consideration, the rotor response to a 90 degree circumferential distortion showed slightly less loss in overall pressure ratio with higher loading. However, increased loading had a deleterious effect on stage performance. The principal portion of the loss in overall stage performance was sustained by the highly loaded stator.

3.2 Rotor - Upstream Flow Interaction

Circumferential distributions of total pressure, static pressure, and axial velocity at the midspan radial position (near stall, design speed) obtained with circumferentially distorted inlet flow to the higher loaded stage (14-10) are shown in Fig. 10. Measurements were taken at three axial locations between screen and rotor. The mid-span distributions of these parameters are considered representative since no notable differences occurred in the spanwise direction. The trends and magnitude are similar to those reported in Ref. 4 for Stage 11-4, and those distributions will not be repeated here.

Fig. 10(a) indicates that no significant change in total pressure distribution occurs in the region between screen and rotor inlet. But there is attenuation of the initial axial velocity distortion (Fig. 10(c)) as the flow approaches the rotor inlet, and magnification of an initially small distortion in static pressure (Fig. 10(b)).

Although there were no notable variations from hub to tip in the foregoing parameters, the absolute tangential velocity did show considerable variation. Fig. 11 compares the tangential velocities obtained for the two stages (Stage 11-4 being taken from Ref. 4). As the flow approaches the rotor, tangential velocity components are induced in the corotating (+) and counter-rotating (-) directions. The induced components are much stronger in the hub region.

A comparison of the distributions for Stage 11-4 (from Ref. 4) and those for Stage 14-10 revealed no significant differences in the distributions nor in the magnitude of the effects. Rotor blade loading does not, therefore, appear to be a significant factor influencing the interaction of the rotor with the upstream distorted flow field.

3.3 Circumferential Flow Distributions

Conventional compressor data analysis is established on the premise of steady, axisymmetric inlet and exit flow conditions. When the inlet flow is circumferentially distorted some important compressor parameters cannot be accurately calculated because:

(1) The rotor relative flow field is unsteady, and

(2) Matching an exit condition to its corresponding condition is uncertain.

Blade element parameters such as diffusion factor, loss coefficient, meridional velocity ratio, and efficiency are therefore not available and, because of the unsteady relative flow field, probably not applicable. Data analysis is consequently directed toward behavior of selected parameters measured or calculated at each axial station, rather than between two stations.

In the interest of brevity only the near stall operating condition at design speed will be discussed for each stage. It should be noted that the flow mechanisms operative at near stall, design speed, are not necessarily representative of flow mechanisms at other flow and speed conditions. However, because of the importance of the stall condition in limiting the operating range of the fan, it is of great interest to investigate flow conditions at near stall with distorted inlet flow.

3.3.1 Rotor Response

Rotor incidence angle distribution is influenced by the induced tangential velocity distribution, the distortion in axial velocity upstream and by blade speed components. For both rotors (Fig. 12) the incidence angle near the hub (90% span from tip) showed the greatest excursion. This can be compared to the incidence angle measured with the backup screen (BUS), and denoted by the solid symbols.

The circumferential distribution of energy addition to the air by the rotor is indicated by the rotor outlet total temperature shown in Fig. 13. (Because inlet temperature is circumferentially constant, exit temperature distribution is representative of temperature rise or temperature ratio.) The outlet temperature is highest in the tip region at the near stall operating condition and shows a greater excursion in the distorted sector above undistorted sector levels than shown at other radial positions. This occurs because the changes in axial velocity cause relatively larger changes in outlet tangential velocity (and therefore energy addition) in the tip region. The rotor tip energy addition is more responsive even though circumferential variation of incidence angle is relatively small.

It is of interest to note that the total pressure distribution behind the rotors shown in Fig. 14 follows the general trend of energy addition (total temperature, Fig. 13) as the blading enters the distorted sector ($\theta = 135^{\circ}$). (Note that exit total pressure distribution is not necessarily proportional to pressure rise or loading because the inlet total pressure distribution is not circumferentially constant.) The total pressure increases as the temperature increases and as the temperature exceeds the uniform inlet stall condition (BUS). Beyond this point the total temperature behind the rotor tip region continues to increase while pressure decreases. These distributions seem to indicate that the blade surface boundary layer has separated and local blade stall may have occurred. This appears to be a local dynamic phenomenon because overall stage stall was not noted. After the rotor passes through the distorted sector the total pressure increases, indicating stall recovery, i.e., boundary layer reattachment.

The response of the rotor tip region most clearly demonstrates the unsteady airfoil response characteristics reported in Ref. 7. In the reference experiment a single airfoil oscillated in free stream flow demonstrated that unsteady normal force coefficients (and angle of attack) exceeded steady state limits before airfoil stall was observed. Similar mechanisms apparently are involved in the rotor blading but are further complicated by the variation of flow parameters and geometry along the blade span, and by interaction with wall boundary layers.

Rotors 11 and 14 show similar hub section response to the distortion, but the response differs from that shown by the tip regions. Just inside the screened region at $\theta = 150^{\circ}$ exit total pressure fell below undistorted levels (Fig. 14c). This is consistent with the corotating induced absolute tangential velocity (Fig. 11 at $\theta = 130^{\circ}$), which is also reflected in the total temperature distribution as a decrease in energy addition (Fig. 13). The cause of the decrease in total pressure between $\theta = 175^{\circ}$ and 190° is not clear. If it is a local boundary layer stall, as observed in the tip region, then it is difficult to explain the continuing increase in total pressure to $\theta = 240^{\circ}$. However, the high level of total pressure recorded at $\theta = 240^{\circ}$ is consistent with the high counter-rotating absolute tangential velocities (Fig. 11) and high level of energy addition (Fig. 13).

The net effect of the rotor hub response is an amplification of the distortion magnitude. The tip region effectively attenuates the distortion.

A comparison of BUS values and levels of total temperature with distortion (Fig. 13) shows that less energy was added by the tip and mean regions of the rotor in the undistorted sector than was added in the BUS tests. (A perfect comparison cannot be made because near stall weight flows for BUS and distortion

tests differ slightly, but for purposes of discussion these differences will be ignored herein.) For the circumferential distortion case, redistribution of flow must occur due to the presence of the screen. For the same flow rate for BUS and distorted flow, the unscreened portion of the annulus must pass flow at higher axial velocity than the corresponding BUS level. The increased axial velocity at rotor exit acts to reduce absolute tangential velocity and therefore, energy addition. In fact, the experimental results (Fig. 15) showed an axial velocity acceleration through the rotor in this case. The additional increase in axial velocity, above the amount attributable to screen blockage redistribution, is due to continuity requirements. Because energy addition is lower in the unscreened sector, exit pressure is lower, and consequently density is lower. To maintain the required flow at lower density, axial velocity must increase.

The circumferential and radial distributions of parameters are translated into overall performance by a mass-averaging process. Since axial velocity is greater than average in the undistorted sector, this sector is weighted more heavily in calculating overall performance, and it is in this sector that energy addition and exit total pressure are lower than BUS levels. Therefore, if increased losses are not sustained, it can be expected that lower overall performance will be realized from circumferentially distorted flow simply because of flow redistributions associated with continuity and radial equilibrium requirements. An examination of rotor exit pressure and temperature distributions (Figs. 13 and 14) does not indicate that losses increased in the undistorted sector, but only that energy addition was lower.

3.3.2 Stator Performance

The passage of the rotor through the distorted sector results in an unsteady flow through the rotor passage. The stator, however, operates with a steady, but spatially distorted flow. Some stator blades always operate in the distorted sector while others always operate in the undistorted sector. As in the rotor, radial equilibrium must be satisfied and, in addition, static pressure must be circumferentially constant at some point downstream of the stator in the annulus or plenum.

A representation of stator losses can be obtained from Fig. 16 which shows total pressure distributions at stator inlet and exit stations for each blade element. The distance between the curves represents losses. Solid symbols mark the BUS test values at near stall.

Differences in losses are evident between stators 4 and 10 and account for the differences in stage overall pressure ratio previously noted. Stator 4 shows losses in the undistorted sector at all radial positions to be comparable to losses with BUS. But in the distorted sector (where incidence angles are greater than BUS values) the losses are higher. This implies a viscous loss due to greater boundary layer growth. Distributions for stator 10, the higher loaded stator, are not so clear cut. Tip and mean radial positions show higher losses over a small portion of the distorted sector. At the hub, however, large losses are indicated in the undistorted sector between $\theta = 240^{\circ}$ and 360°. The probable source of these losses is the higher than BUS levels of stator hub inlet Mach number (as high as 0.85) indicated in Fig. 17. It was discussed earlier, and shown in Fig. 6, that because of attempts to prevent stator hub choking the throat area ratio and X-factor (front turning) were increased. This led to large suction surface Mach numbers (1.4) which, in turn, probably leads to high shock losses. This is believed to be the major source of the overall stator performance loss.

The other likely source of stator performance decrements, and also a probable cause of total flow breakdown in the stage, is the increase in viscous loss due to off-design operation at high incidence. This is illustrated in Fig. 18. Plotted in the figure for the tip, mean, and hub sections of stators 4 and 10 are the total loss coefficients calculated from measured data for the BUS tests. It is evident at once that, except for the mean section, stator 4 performed at design levels near zero incidence (design incidence), but that stator 10 sustained higher than design losses at tip and hub sections, and hub section losses were particularly high. Plotted above each figure is a line for each stator which represents the range of stator incidence angles, from minimum to maximum, for circumferentially distorted flow (see sketch on the figure for definitions). A circle on each line represents the average value that blades in the undistorted sector experience. The cross-hatched length is the range of incidence angles which a 90 degree sector of the stator experiences (corresponding roughly to the distorted sector). It is clear that in all blade regions incidence angle over much of the distorted sector exceeded the incidence angle which corresponds to stall conditions for BUS tests. Because loss increases with incidence and because the level of loss is already very high in the stator 10 hub, conditions in the stator hub were conducive to a locally stalled flow.

4.0 CONCLUDING REMARKS

Two transonic fan stages having different design pressure ratios were tested with a 90-degree circumferential distortion imposed on the inlet flow. Both fan rotors had nominal tip diameters of 50.8 cm, design tip speeds of 425 m/sec, design equivalent weight flows of 29.5 kg/sec, and hub-to-tip radius ratios of 0.5.

The lower loaded stage (designated Stage 11-4) was designed for a stage overall pressure ratio of 1.57 and the stage designated 14-10 was designed for a 1.75 pressure ratio. Circumferential distortion data were obtained at 100 and 70 percent of design speed. At design speed the magnitude of distortion (defined by a $(P_{max} - P_{min})/P_{max}$ parameter evaluated at mid span) was 0.12 and at 70 percent of design speed the magnitude was between 0.04 and 0.045. Overall performance was obtained and detailed flow parameters were measured at three radial positions at several axially located measuring stations. Performance with circumferential distortion for each stage was compared; and distortion performance for each stage was also compared to performance measured with only the support screen in place (undistorted flow).

At design speed, both rotors 14 and 11 showed losses in overall pressure ratio due to distortion. However, the higher loaded rotor (14) showed a slightly lower loss. Conversely, comparing complete stage performance, the higher loaded stage sustained the greatest loss in overall pressure ratio at design speed, which indicates the stator as source of the performance loss. Due to the small magnitude of the distortion at 70 percent of design speed (near stall), no significant loss in overall pressure ratio was recorded ex-

cept through stator 10.

The principal difference in response to a circumferential distortion between the two stages was attributable to differences in stator flow. Because inlet flow to the stator is spatially distorted, the loss in performance was due to a steady state phenomenon. Circumferential flow redistribution, due to the presence of the screen, produced higher flow and axial velocity through the undistorted sector, raising inlet and blade suction surface Mach numbers in the stator hub region. This produced greater shock losses in stator 10 than were sustained in distortion-free tests.

This experience points up the need for attention to the selection of stator blade profiles in the design process. Increased stage loading does lead to high stator hub Mach numbers and circumferentially distorted flow also leads to higher Mach numbers in the undistorted sector as a result of flow redistribution. Thus, as stage loading increases, the stator hub region is susceptible to increased shock losses when operating in circumferentially distorted flow. If care is taken to design highly loaded stators by incorporating blade shapes with higher critical Mach numbers, less loss in performance and greater operating range with distortion may result.

Overall pressure ratio was also lower than BUS levels in both rotors, but is not necessarily attributable to dynamic effects. In each rotor less energy was added by the upper half of the blade in the undistorted sector of flow than was achieved in BUS tests. The lower energy addition and realized pressure ratio appears to be a direct result of flow redistributions of the circumferentially distorted flow dictated by continuity requirements. The decrement in rotor performance between undistorted flow tests and circumferential distortion tests appears to be due principally to lower energy addition and not to increased losses.

At near stall conditions the (unsteady) response of the rotor blading to a circumferential distortion differed across the span. In the tip region, as the blading passed circumferentially through the distorted sector, an increasing amount of energy was added to the air due to increasing incidence angle and decreasing axial velocity. Total pressure also increased in similar fashion through part of the distorted sector, but then decreased as losses, believed to be associated with suction surface boundary layer separation, increased. After passing through the distorted sector, total temperature and pressure readjusted to undistorted sector levels. In the hub region the total pressure showed a similar, but mild, pattern of increase and decrease, but then increased to greater than undistorted levels. The net effect of the response characteristics of different sections of the rotor at near stall was that the tip region attenuated the magnitude of total pressure distortion while the hub region amplified it. Both rotors demonstrated the same type of span-wise behavior.

Interaction between the rotor and the upstream distorted flow field was recorded for both stages. The distortion in total pressure remained unchanged as the flow approached the rotor while the distortion in axial velocity was attenuated, a distortion in static pressure was amplified, and tangential velocity components were induced (differing radially in magnitude). No influence of loading level on the strength of interaction was noted.

REFERENCES

1. J. P. Gostelow, K. W. Krabacher, and L. H. Smith, Jr., National Aeronautics and Space Administration. Performance Comparisons of High Mach Number Compressor Rotor Blading. 1968, NASA CR-1255.

2. G. Kovich, R. D. Moore, and D. C. Urasek. National Aeronautics and Space Administration. Performance of Transonic Fan Stage with Weight Flow Per Unit Annulus Area of 198 Kilograms Per Second Per Square Meter (40.6 (lb/sec)/ft^2). 1973, NASA TM X-2905.

3. D. C. Urasek, R. D. Moore, and W. M. Osborn. National Aeronautics and Space Administration. Performance of a Single-Stage Transonic Compressor with a Blade-Tip Solidity of 1.3. 1972, NASA TM X-2645.

4. N. L. Sanger. Performance of a 1.57 Pressure Ratio Transonic Fan Stage with a Screen-Induced 90° Circumferentially Distorted Inlet, Proposed NASA TN.

5. D. C. Urasek and D. C. Janetzke. National Aeronautics and Space Administration. Performance of a Tandem-Bladed Transonic Compressor Rotor with Tip Speed of 1375 Feet Per Second. 1972, NASA TM X-2484.

6. G. E. Glawe, L. N. Krause, and T. J. Dudzinski. National Aeronautics and Space Administration. A Small Combination Sensing Probe for Measurement of Temperature, Pressure, and Flow Direction. 1968, NASA Publication TN D-4816.

7. F. O. Carta. Unsteady Normal Force on an Airfoil in a Periodically Stalled Inlet Flow. J. Aircraft, Vol. 4, no. 5, Sept-Oct. 1967, pp. 416-421.

TABLE I. - DESIGN PARAMETERS FOR STAGES 11-4 AND 14-10

	Stage 11-4	Stage 14-10
Rotor pressure ratio	1.60	1.80
Stage pressure ratio	1.57	1.75
Rotor temperature ratio	1.16	1.21
Stage temperature ratio	1.16	1.21
Equivalent flow rate, kg/sec	29.48	29.48
Rotor tip speed, m/sec	425	423
Diffusion factor, rotor tip	0.43	0.54
Diffusion factor, stator hub	0.48	0.54
Solidity, rotor tip	1.30	1.30
Solidity, stator tip	1.27	1.30
Aspect ratio, rotor	2.5	2.4
Aspect ratio, stator	2.4	2.0
Rotor tip radius at inlet, cm	25.20	25.08

TABLE II. - SUMMARY OF EFFECT OF CIRCUMFERENTIAL DISTORTION ON STALL PRESSURE RATIO FOR STAGES 11-4 AND 14-10

		Stage 11-4		Stage 14-10	
		100% N	70% N	100% N	70% N
Rotor	PR at near stall, BUS	1.70	1.29	1.87	1.36
	PR at near stall, circumferentially distorted	1.60	1.29	1.81	1.37
	ΔPR_S	.06	0	.03	-.01
Stage	PR at near stall, BUS	1.64	1.26	1.77	1.32
	PR at near stall, circumferentially distorted	1.56	1.27	1.64	1.28
	ΔPX_S	.05	-.01	.07	.03

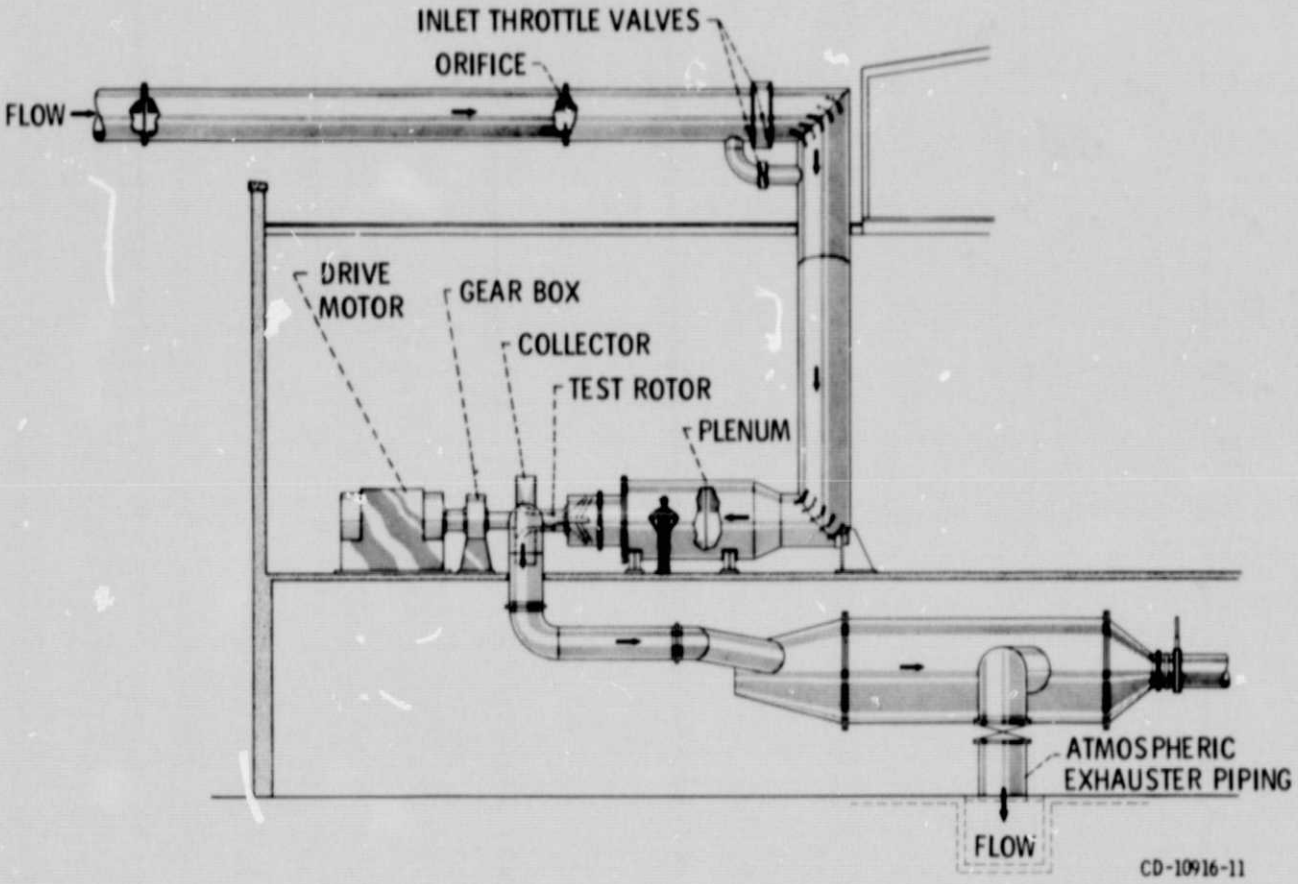

E-8385

Figure 1. - Test facility.

FLOW PATH COORDINATES		
AXIAL DISTANCE, Z, cm	RADIUS r, cm	
	INNER	OUTER
-35.560	7.302	25.400
-30.480	7.302	
-25.400	7.493	
[a]-22.860	7.874	
-20.320	8.255	
-15.240	9.144	
-12.700	9.589	
[a]-10.480	10.050	
-10.160	10.096	
-7.620	10.515	
-5.080	11.049	
[a]-2.540	11.747	
0	12.668	25.336
4.064	13.970	24.638
[a]5.080	14.336	24.460
7.620	14.732	24.384
10.973	15.240	
[a]12.700		
15.240		
17.780		
20.320		

[a]MEASURING STATION.

FLOW PATH COORDINATES		
AXIAL DISTANCE, Z, cm	RADIUS r, cm	
	INNER	OUTER
-30.480	7.303	25.400
-25.400	7.493	
[a]-22.860	7.874	
-20.320	8.255	
-15.240	9.144	
[a]-10.480	10.050	
-10.160	10.097	
-5.080	10.922	
[a]-2.540	11.659	
0	12.668	25.273
4.572	14.605	24.511
[a]6.096	15.240	24.397
7.620	15.748	24.384
11.176	16.510	
[a]13.462		
15.240		
20.320		

[a]MEASURING STATION.

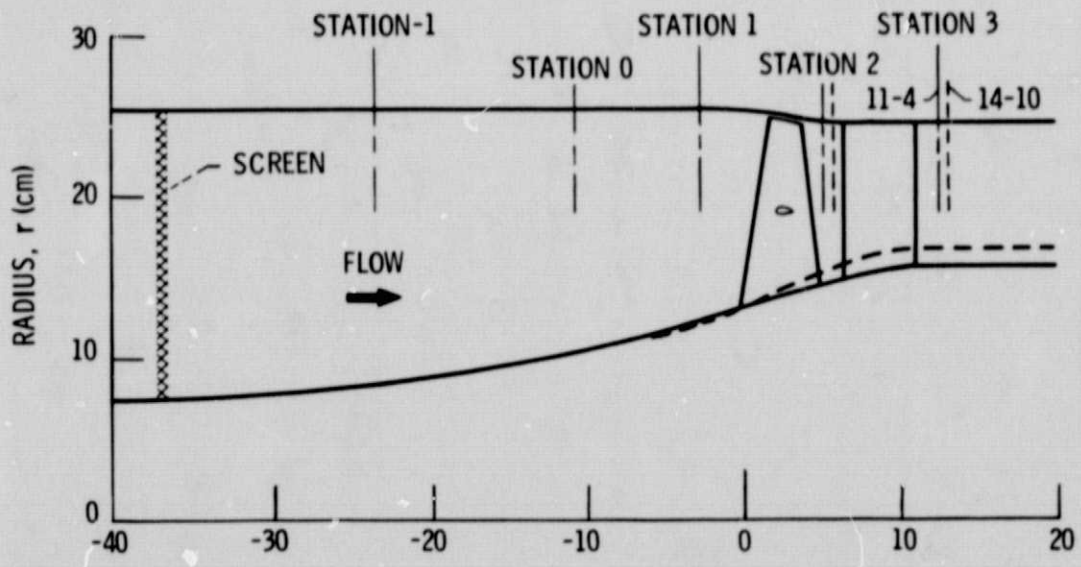

Figure 2. - Flow path schematic for stages 11-4 and 14-10.

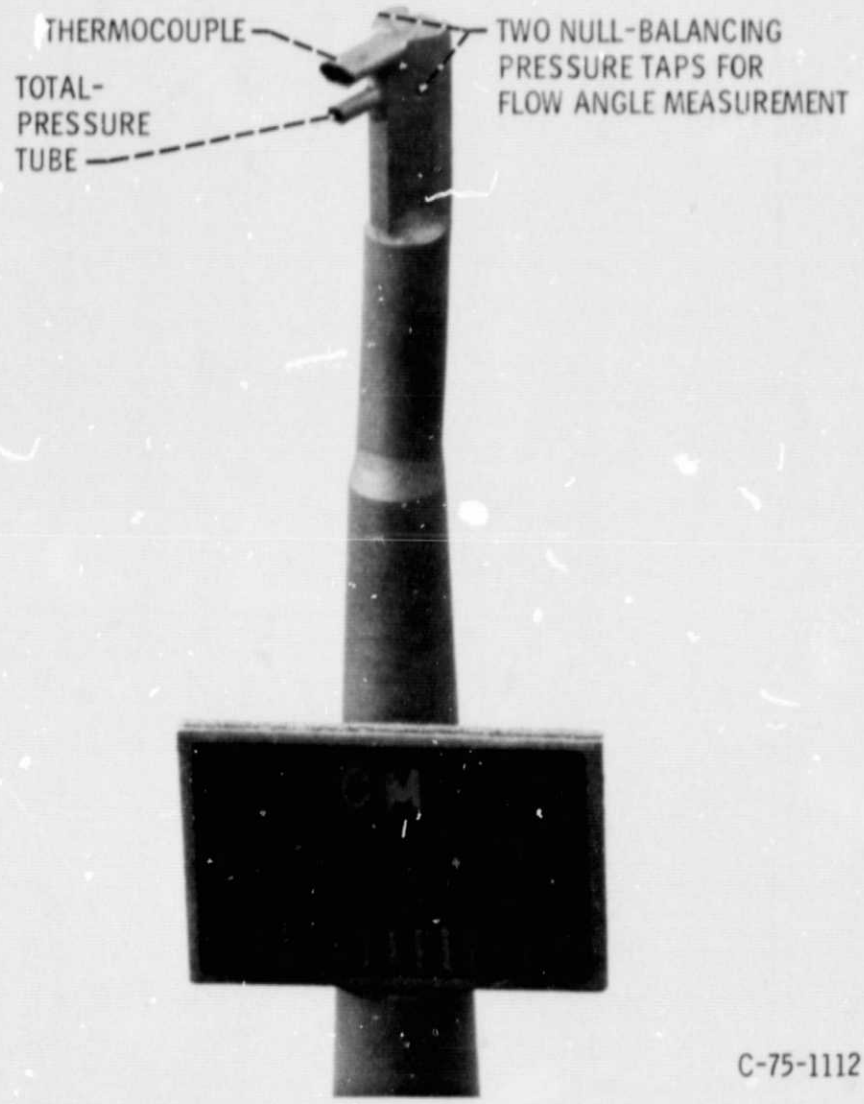

E-8385

Figure 3. - Combination total pressure, total temperature, and flow angle probe (double barrel).

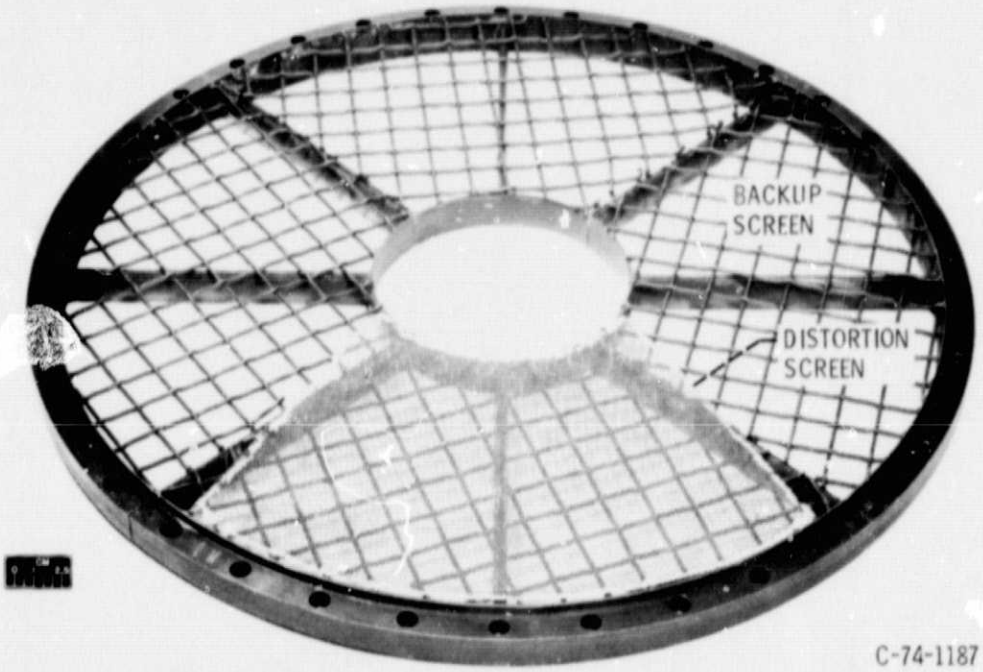

C-74-1187

Figure 4. - Distortion screen and backup screen assembly.

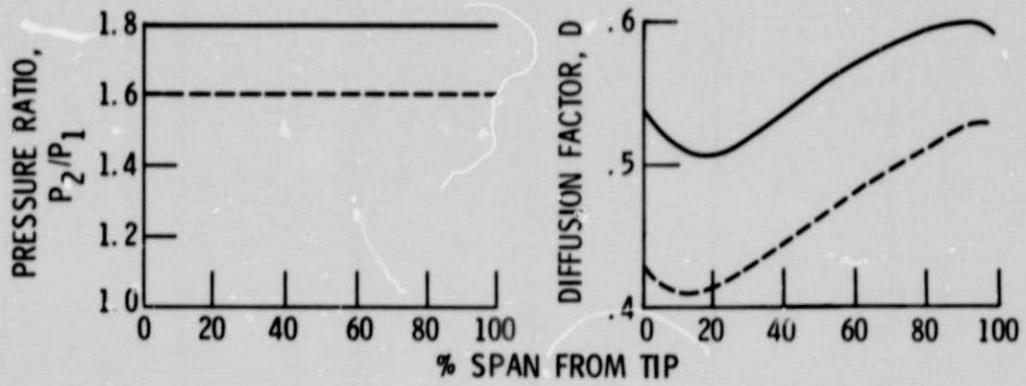

(a) PRESSURE RATIO.

(b) DIFFUSION FACTOR.

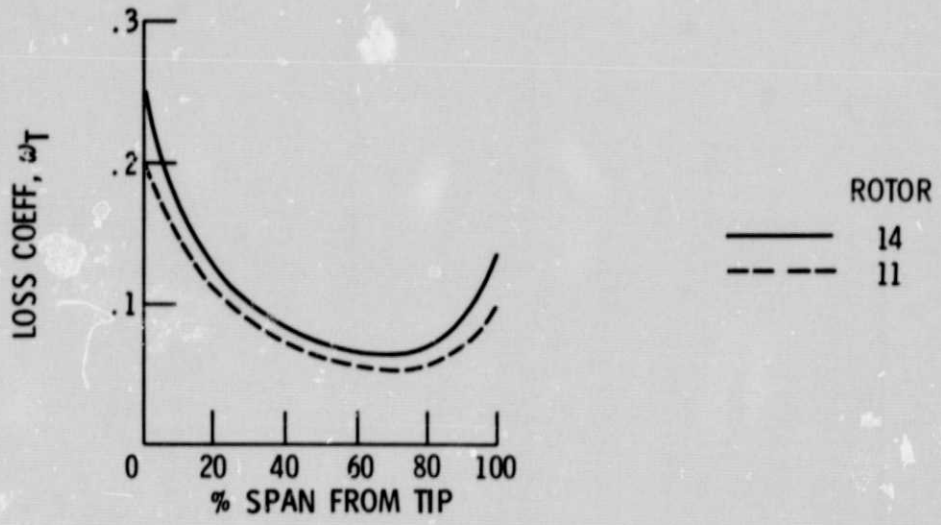

(c) LOSS COEFF.

Figure 5. - Radial distributions of design parameters for rotors 11 and 14.

E-8385

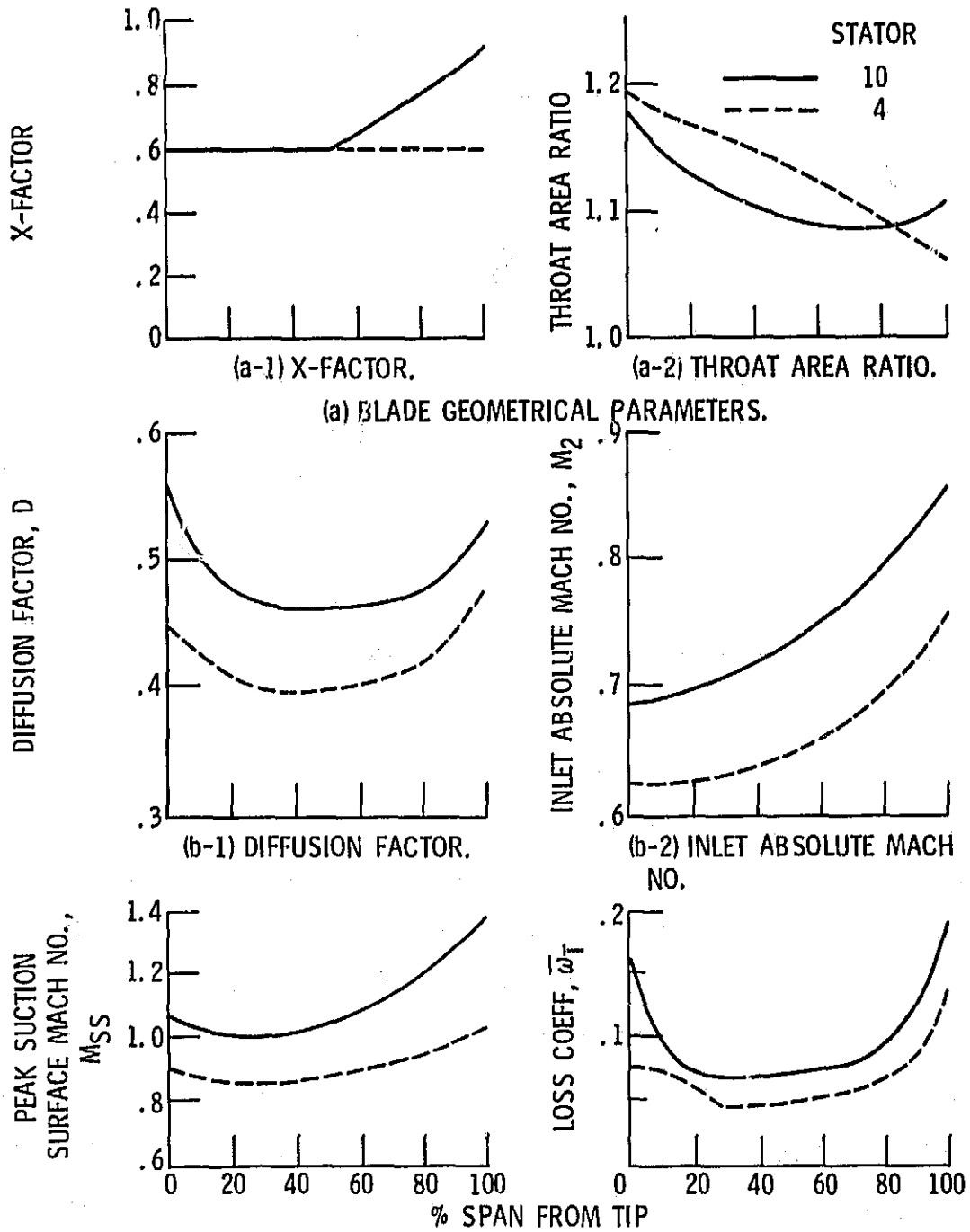

Figure 6. - Radial distributions of design parameters for stators 4 and 10.

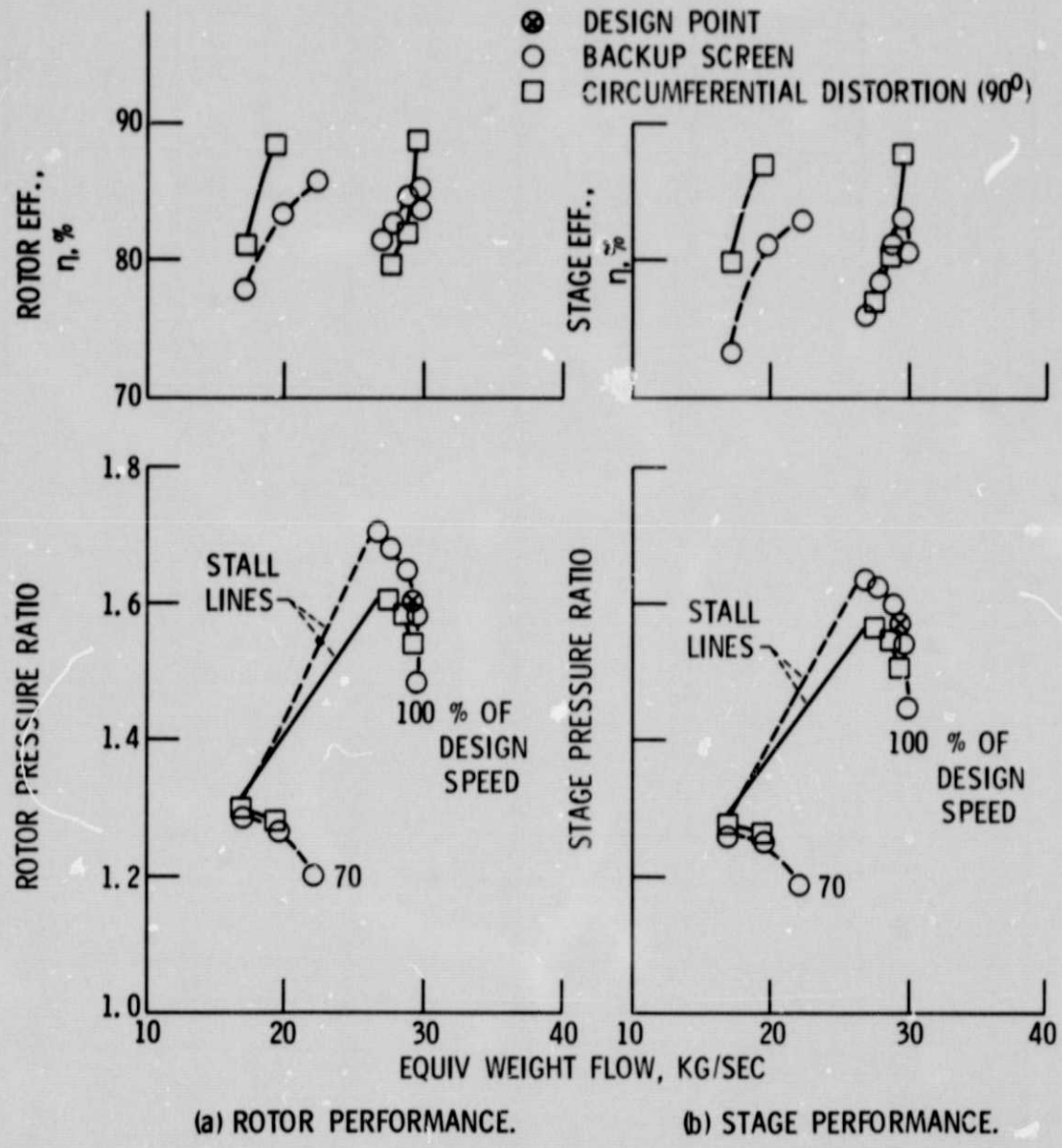

Figure 7. - Rotor 11 and stage 11-4 overall performance, distorted and undistorted inlet flow.

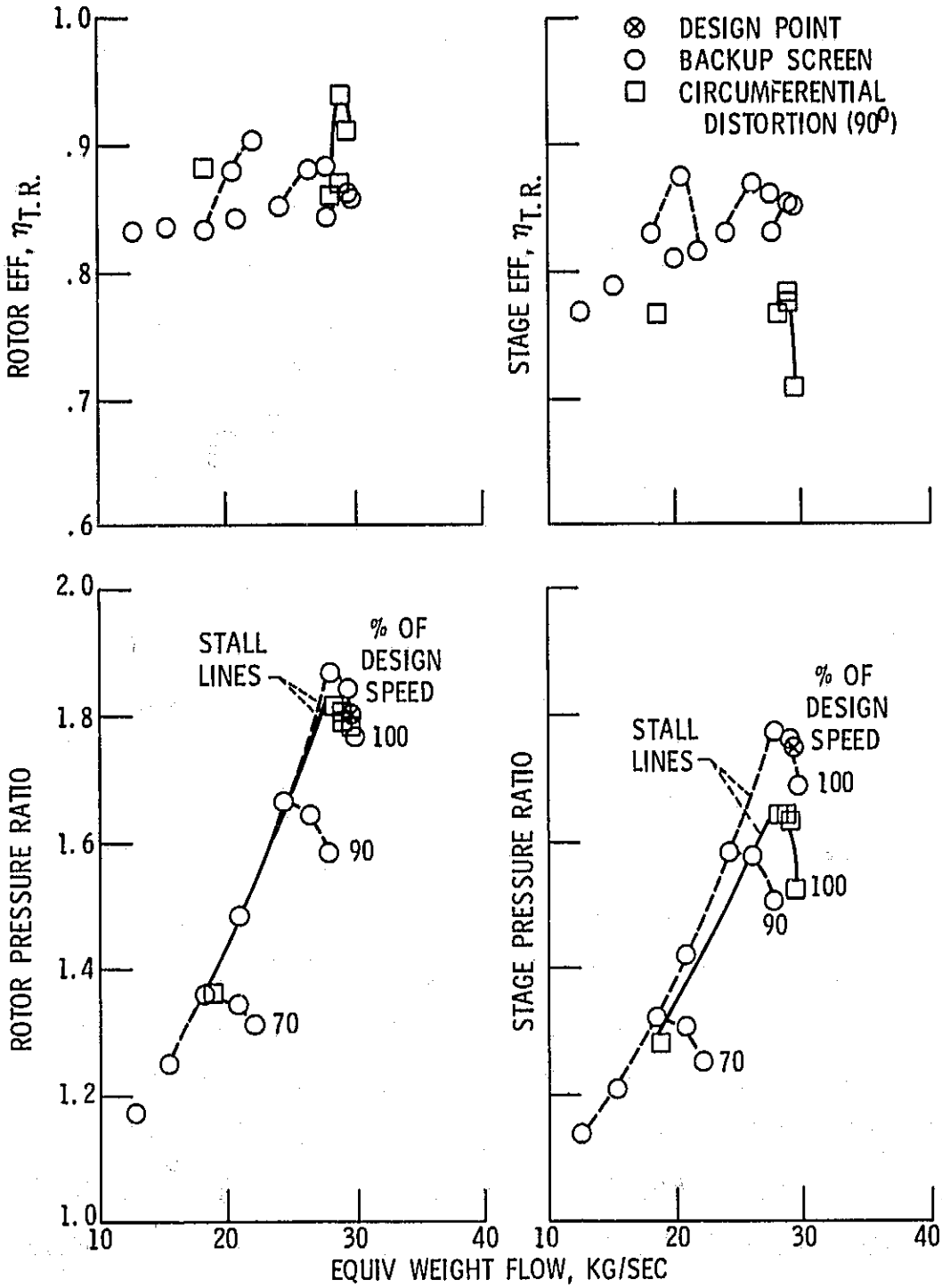

(a) ROTOR PERFORMANCE. (b) STAGE PERFORMANCE.

Figure 8. - Stage 14-10 overall performance, distorted and undistorted inlet flow.

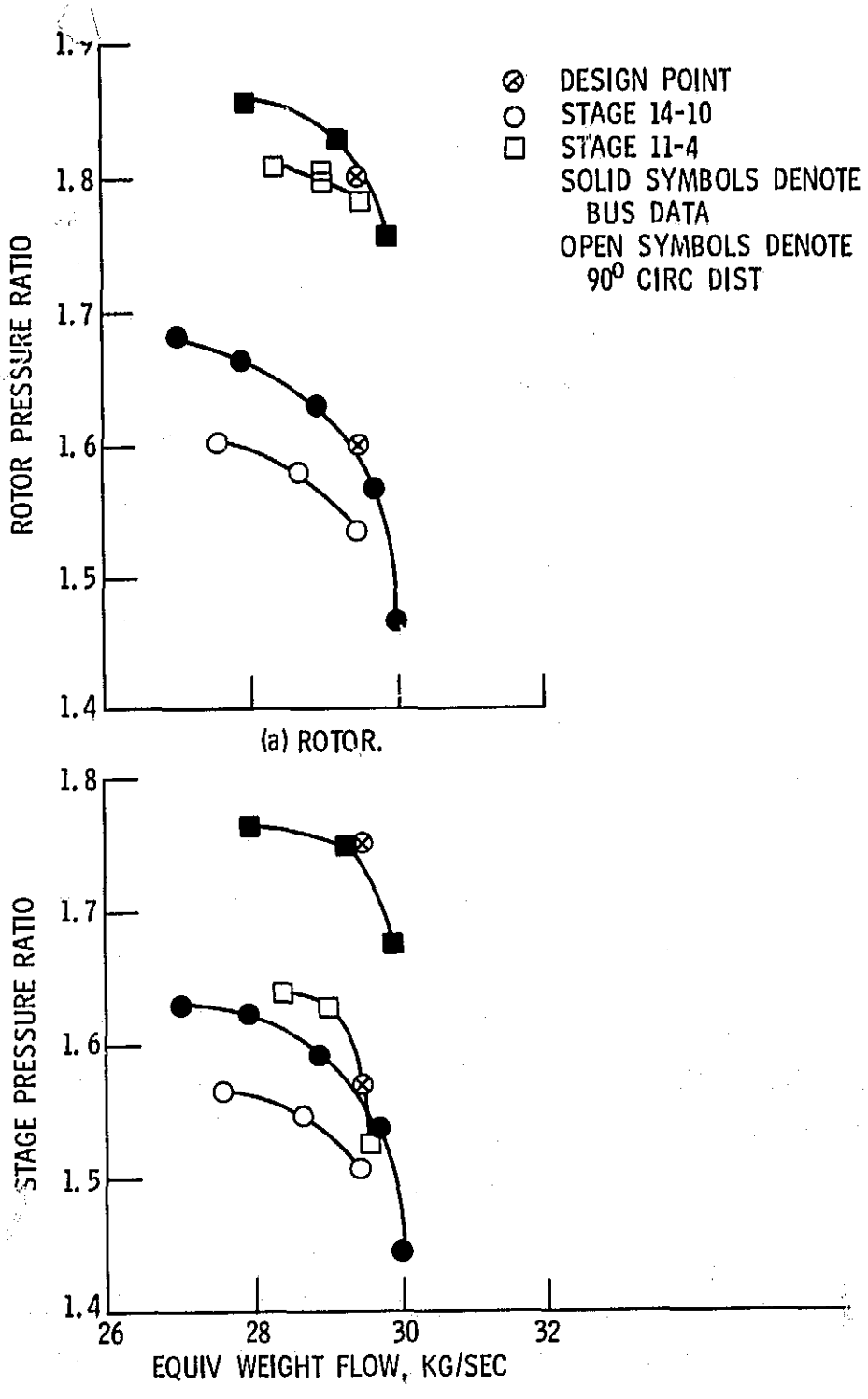

Figure 9. - Comparison of overall pressure ratios for stages 14-10 and 11-4. 100 Percent design speed. Distorted and undistorted inlet flow.

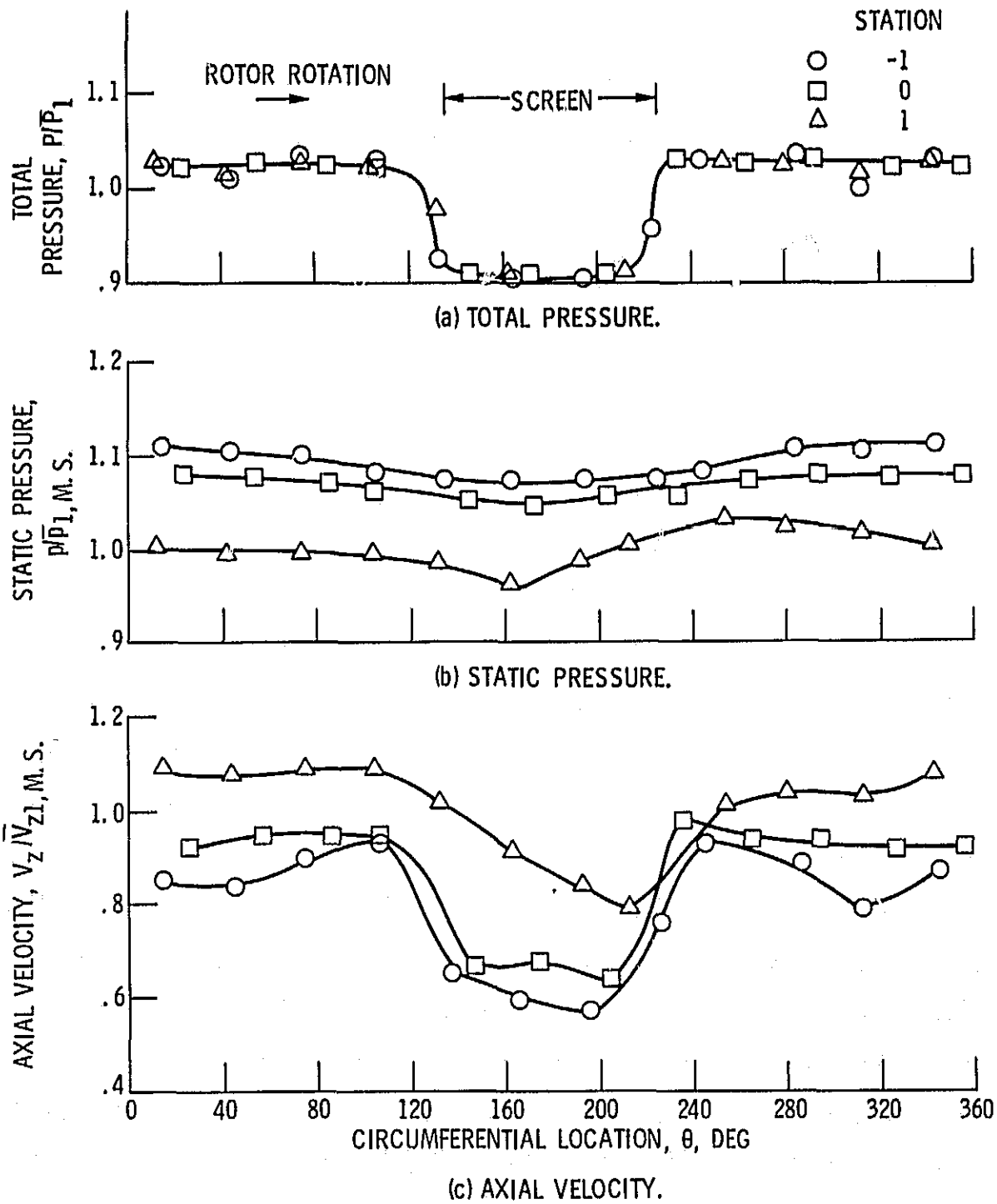

Figure 10. - Circumferential distributions of flow parameters between screen and rotor. Stage 14-10. Near stall. Design speed.

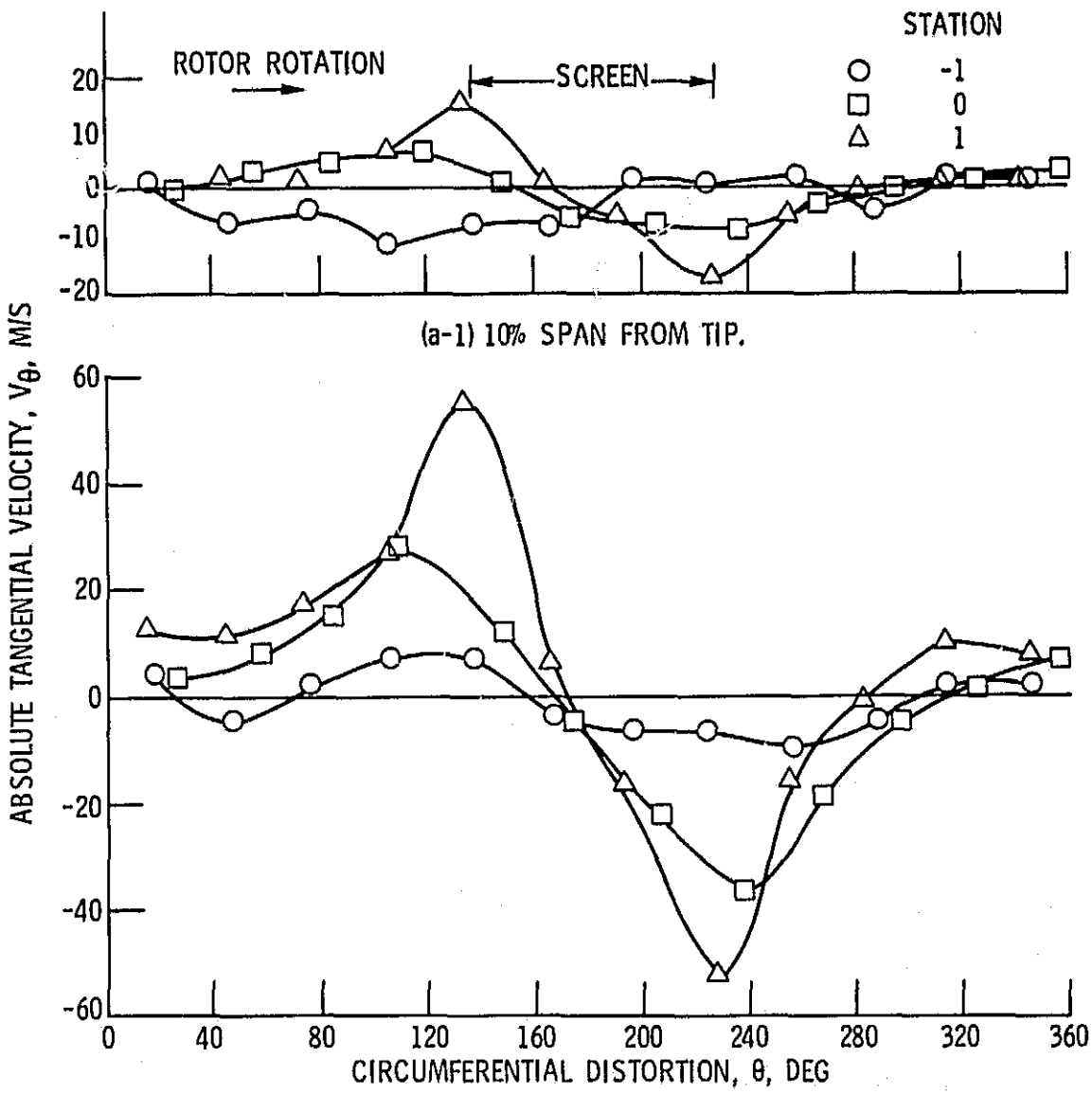

(a-1) 10% SPAN FROM TIP.

(a-2) 90% SPAN FROM TIP.

(a) STAGE 11-4.

Figure 11. - Circumferential distributions of absolute tangential velocity between screen and rotor. Near stall. Design speed.

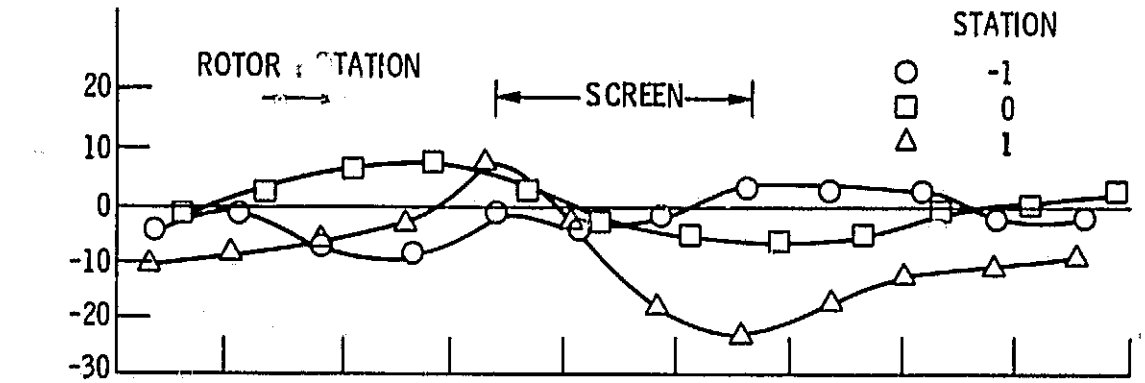

(b-1) 10% SPAN FROM TIP.

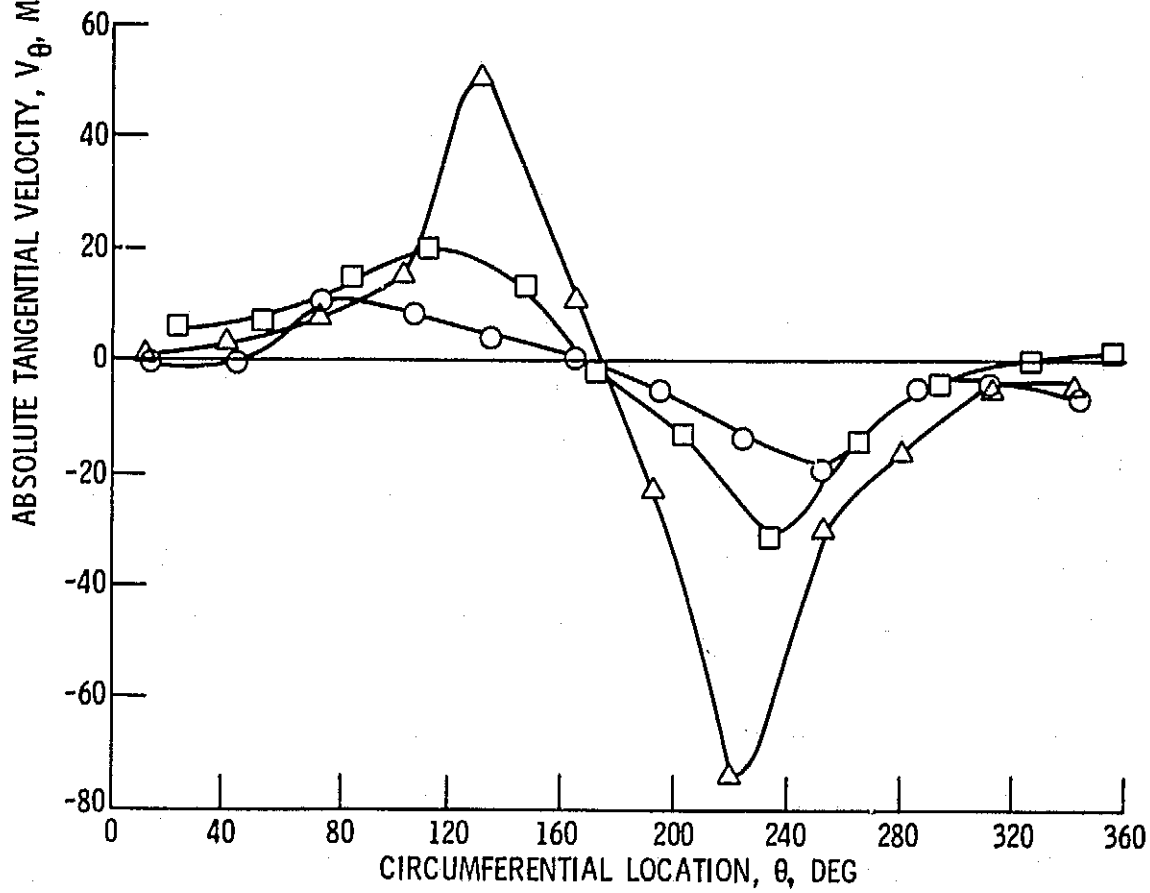

(b-2) 90% SPAN FROM TIP.

(b) STAGE 14-10.

Figure 11. - Concluded.

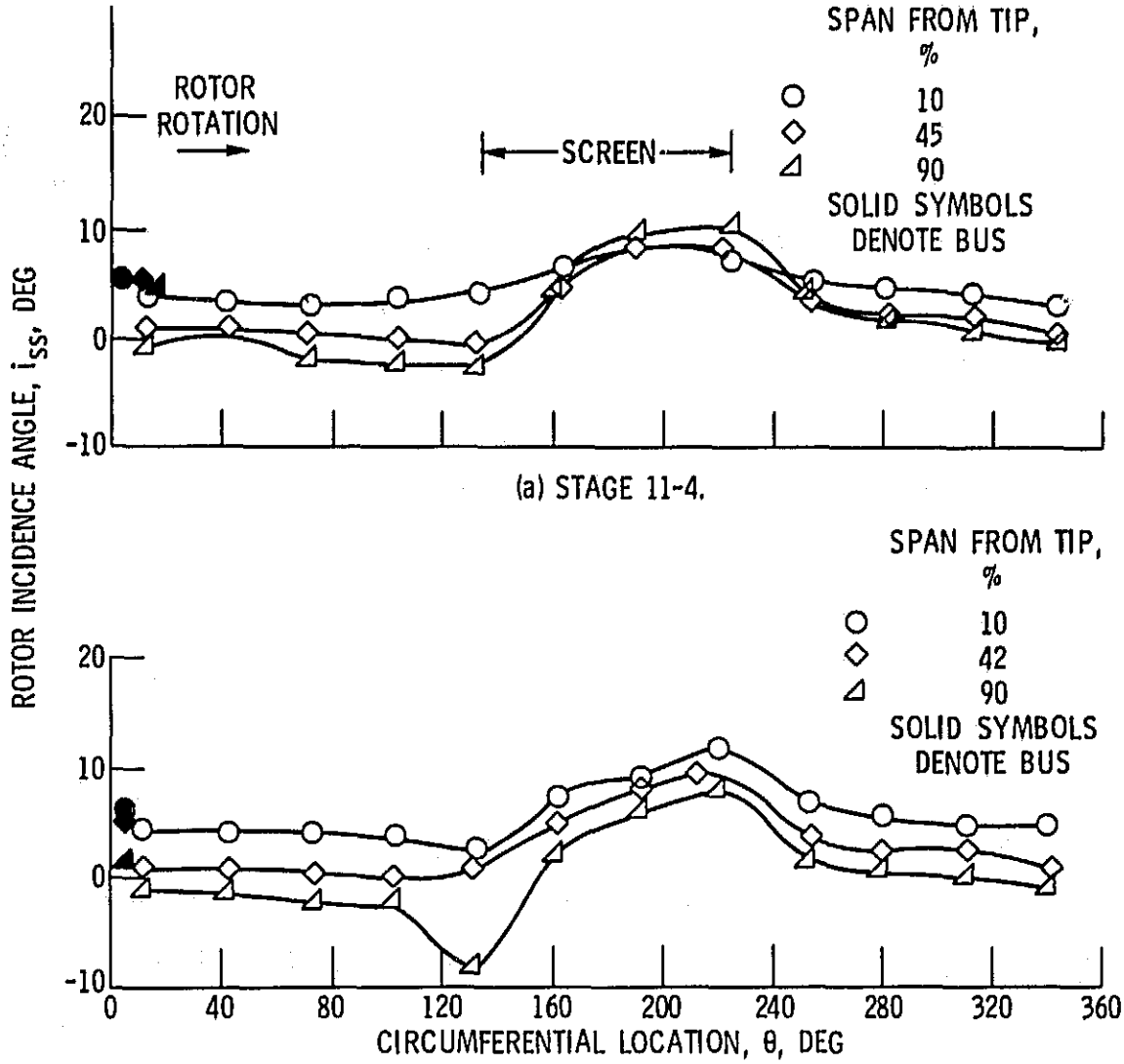

(a) STAGE 11-4.

(b) STAGE 14-10.

Figure 12. - Circumferential distributions of rotor incidence angle for stages 11-4 and 14-10. Near stall. 100% design speed.

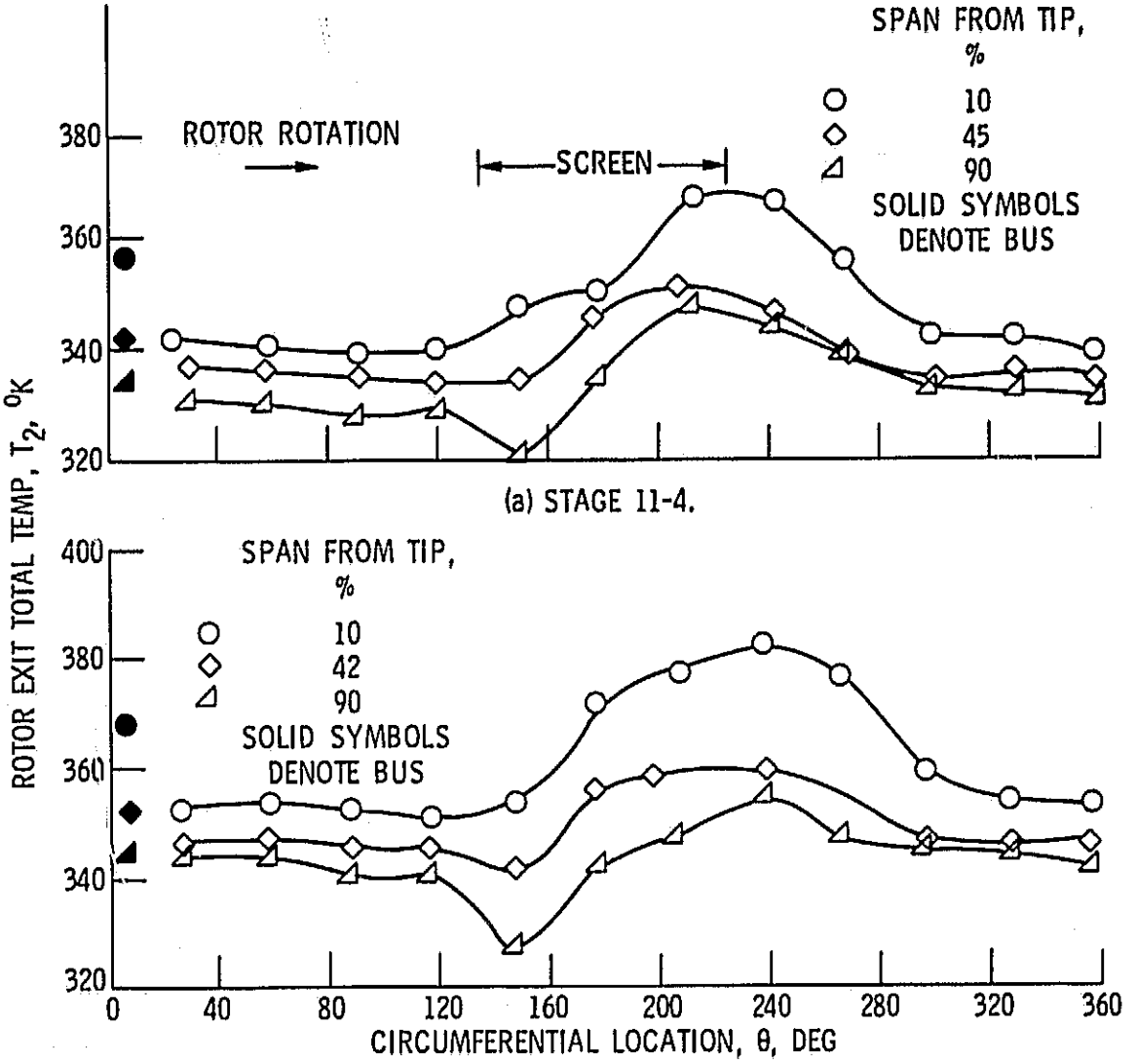

Figure 13. - Circumferential distributions of rotor exit total temperature for stages 11-4 and 14-10. Near stall. 100% design speed.

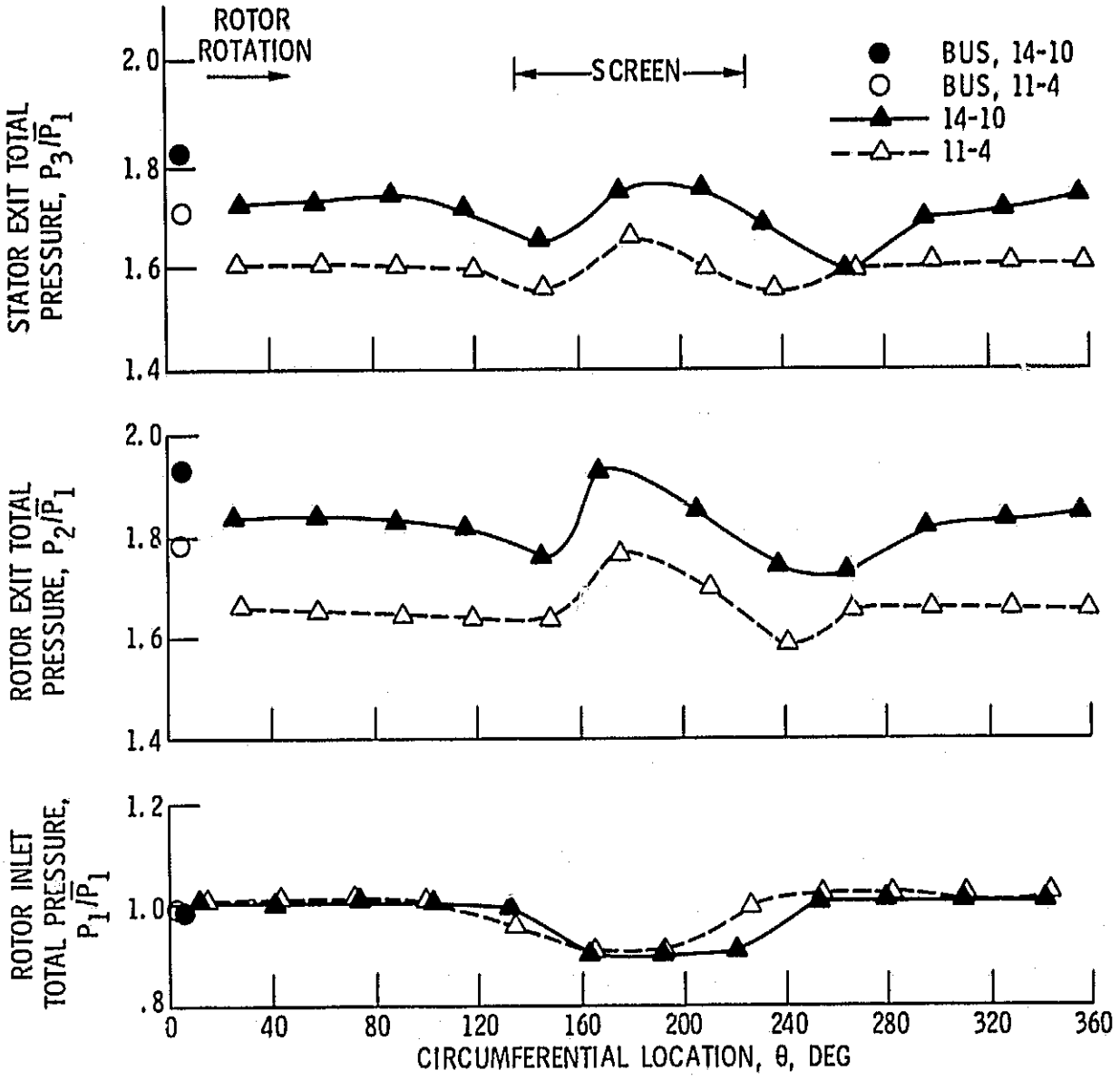

(a) TIP REGION: 10% SPAN FROM TIP.

Figure 14. - Comparison of circumferential distributions of total pressure at rotor inlet, exit, and stator exist for stages 11-4 and 14-10. Near stall condition. Design speed.

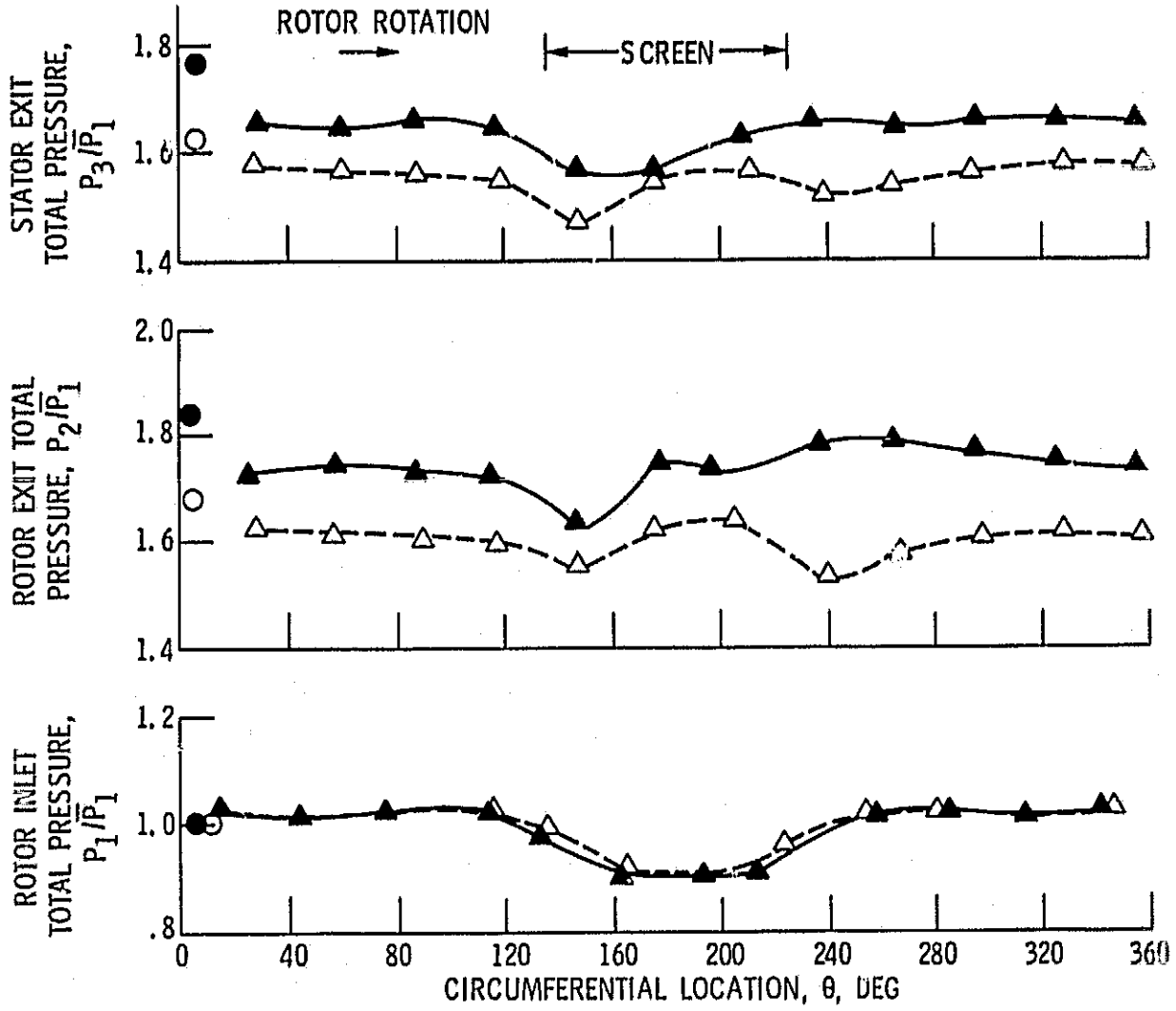

(b) MID SPAN REGION: 45% SPAN FROM TIP (STAGE 11-4); 42% SPAN FROM TIP (STAGE 14-10).

Figure 14. - Continued.

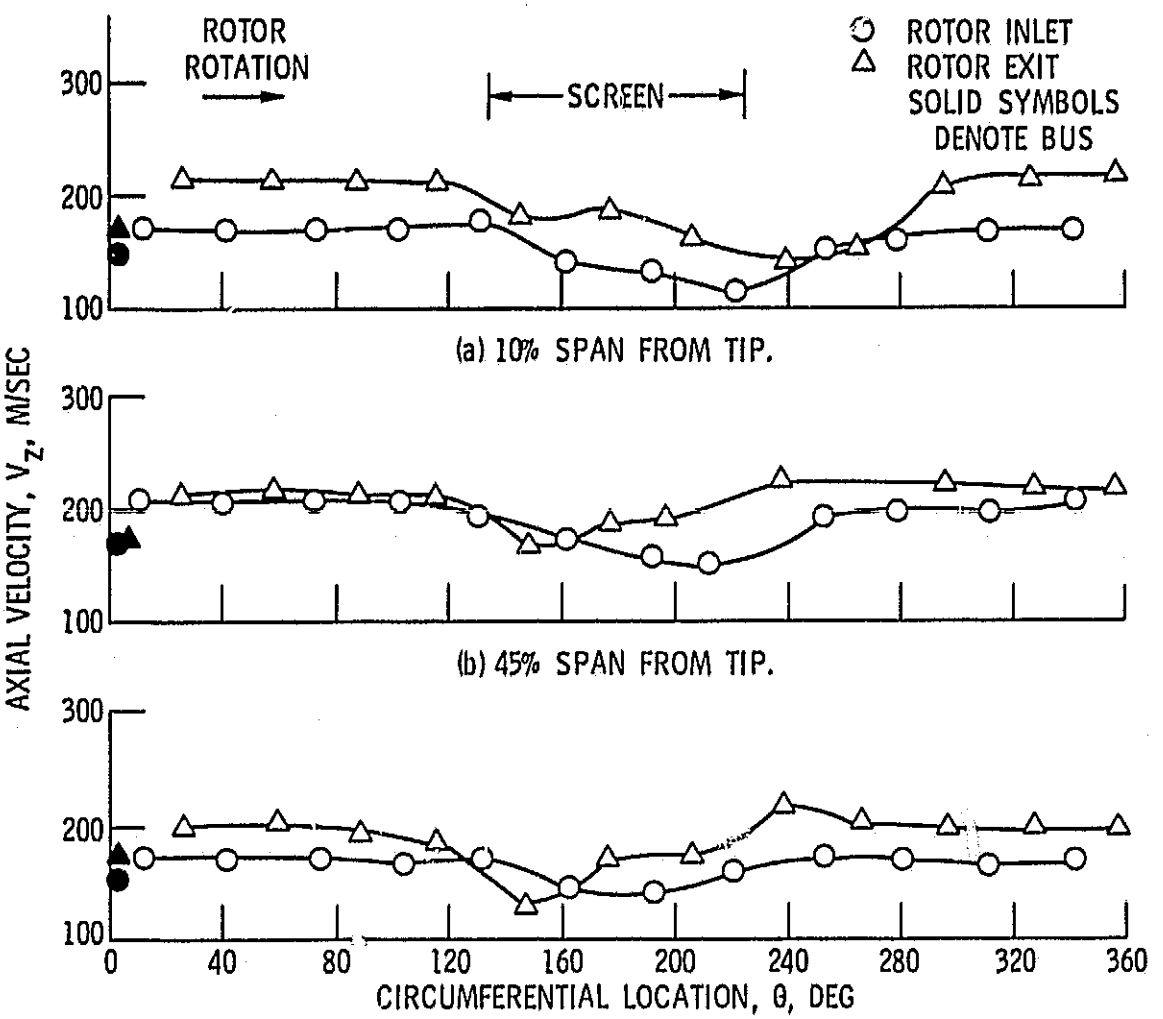

(a) 10% SPAN FROM TIP.

(b) 45% SPAN FROM TIP.

(c) 90% SPAN FROM TIP.

Figure 15. - Circumferential distributions of axial velocity at rotor inlet and exit. Stage 14-10. Near stall. Design speed.

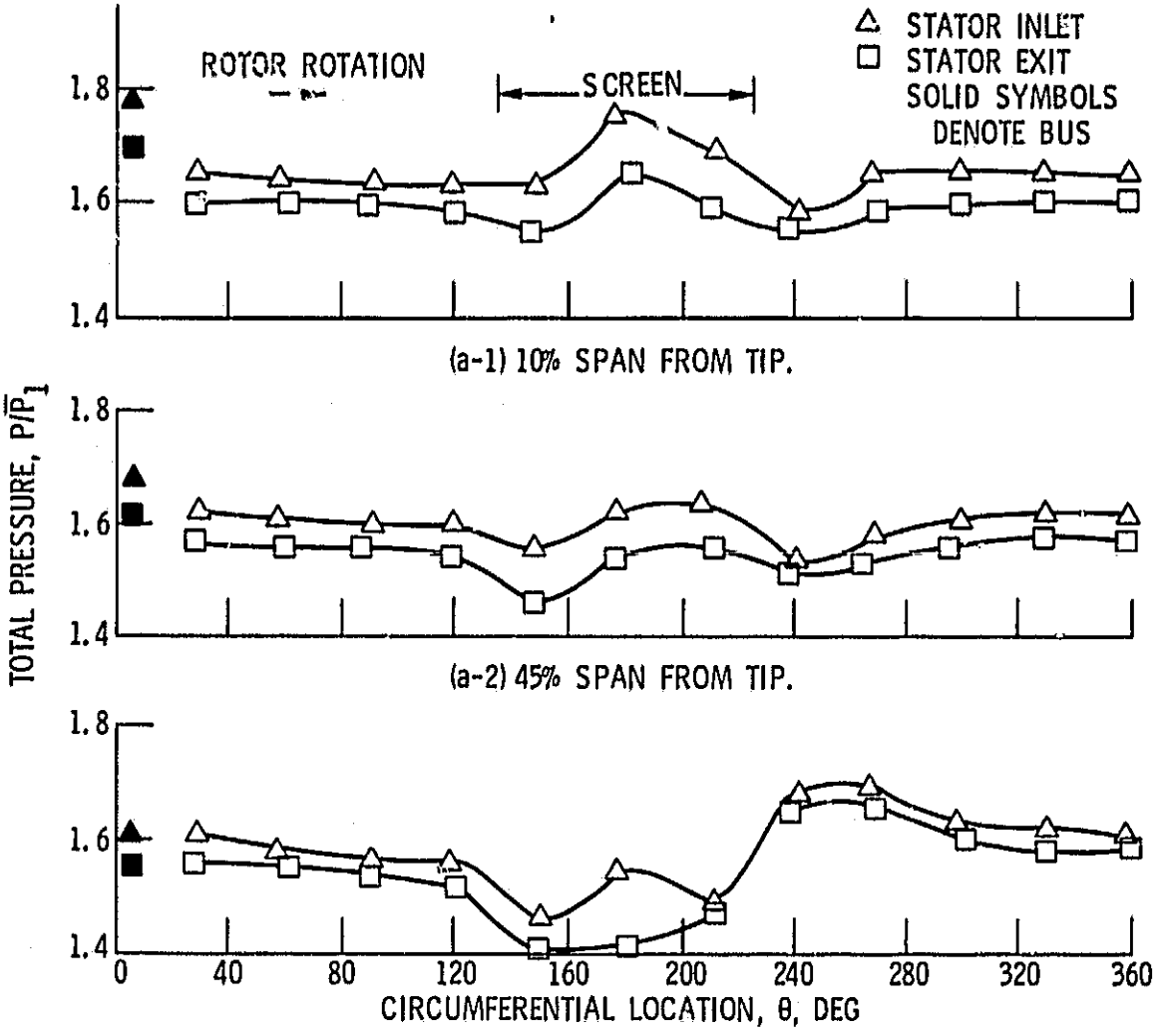

(a-1) 10% SPAN FROM TIP.

(a-2) 45% SPAN FROM TIP.

(a-3) 90% SPAN FROM TIP.

(a) STAGE 11-4.

Figure 16. - Circumferential distributions of total pressure at stator inlet and exit. Near stall. Design speed.

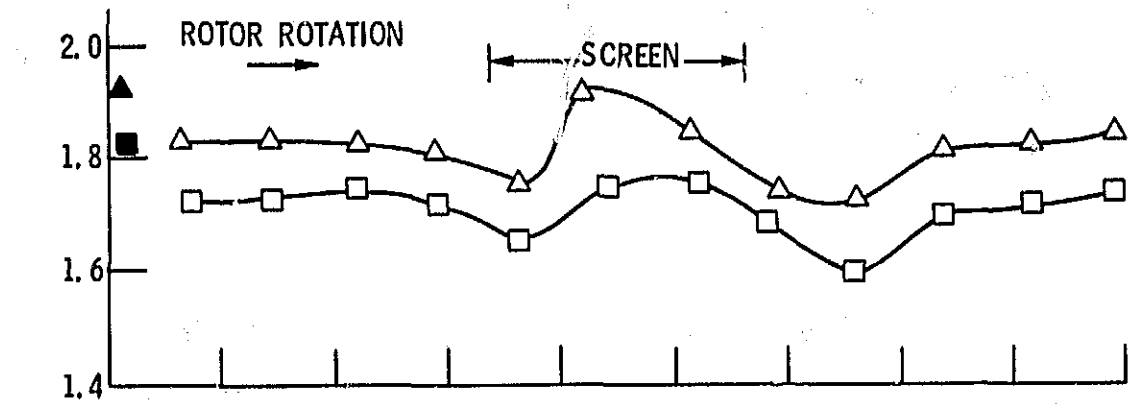

(b-1) 10% SPAN FROM TIP.

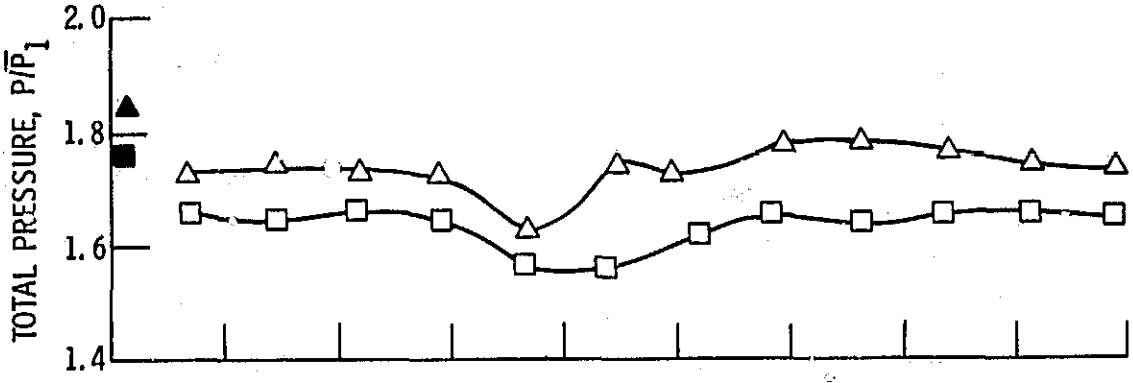

(b-2) 42% SPAN FROM TIP.

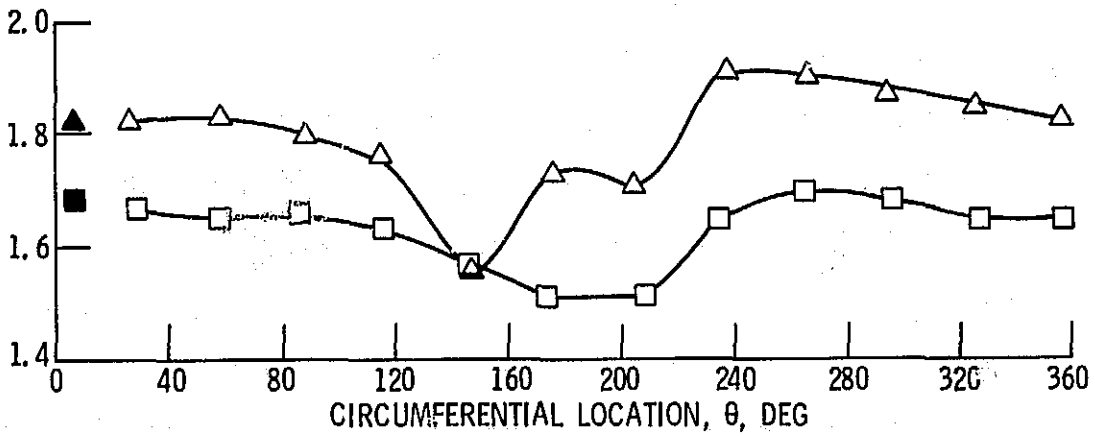

(b-3) 90% SPAN FROM TIP.

(b) STAGE 14-10.

Figure 16. - Concluded.

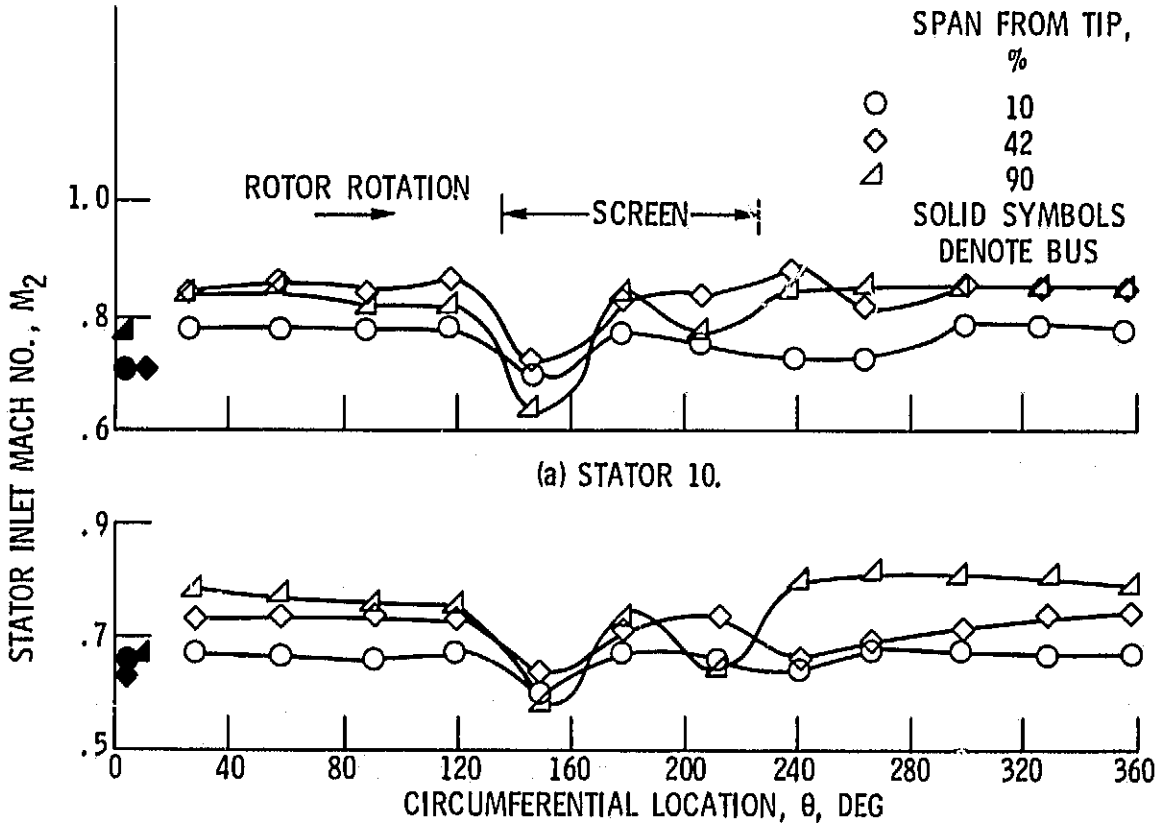

Figure 17. - Circumferential distributions of stator inlet Mach number. Near stall. Design speed.

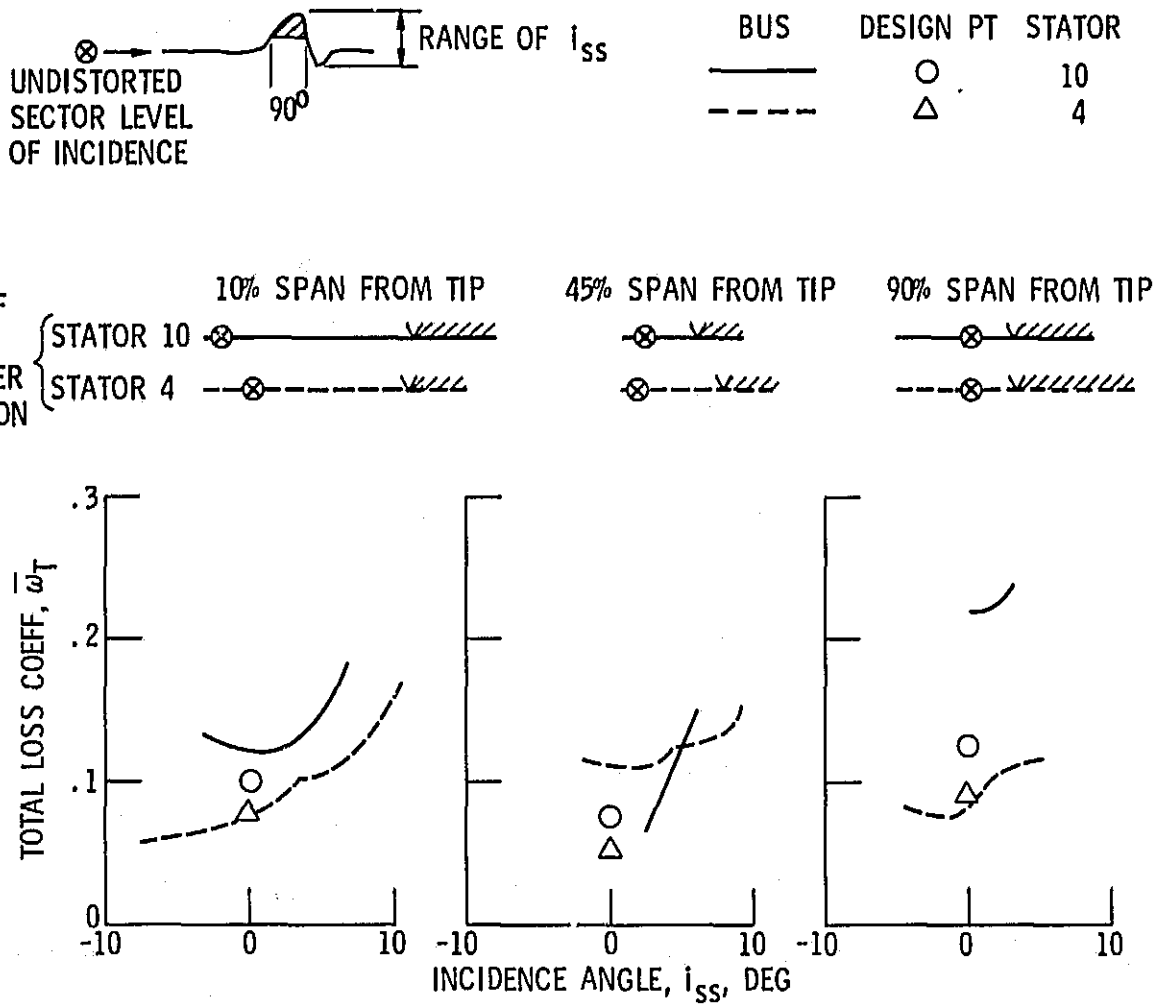

Figure 18. - Stator loss coefficient variation with incidence angle at three radial positions.

E-8385

NASA-Lewis-Com'l